Observations of reservoir quality alteration in proximity to igneous intrusions for two distinct sandstones in Scotland

M. DUFFY*[1], N.J.C. FARRELL[1], R. RAESIDE[1], D. K. MUIRHEAD[1], D. HEALY[1], A. T. BRASIER[1], N. SCHOFIELD[1].

[1]*Department of Geology and Petroleum Geology, School of Geosciences, University of Aberdeen, Aberdeen AB24 3UE, UK*

**Corresponding author (e-mail: m.duffy@abdn.ac.uk)*

Keywords: sandstone, intrusion, porosity, permeability, reservoir quality, thermal alteration

Word Count: 9230

ABSTRACT:

Igneous intrusions are common features within rifted sedimentary basins. With advances in technology, exploration has progressed into more complicated petroleum systems where sediments are segmented and altered by networks of dykes and sills. Magmatism increases temperatures and fluid pressures within adjacent sedimentary host rocks. This can lead to mobilisation of mineral-rich hot fluids through pores and fractures, which alters the host rock microstructure via both mineralisation and dissolution. However, few studies have quantified the impact of intrusions on reservoir quality, specifically on host rock pore networks and their ability to conduct fluid. This study uses a combination of plug porosity and permeability, optical, SEM and cathodoluminescence microscopy and XRD to investigate the mineralogical and reservoir quality changes to sandstones within thermal aureoles. In contrast to published models, associating igneous bodies with reduction of reservoir quality in the host rock, our analyses of two intruded sandstones show that alteration and mobilisation of pore filling minerals and clays can also result in enhancement of porosity and permeability at the intrusion-host rock contact. This study identifies the microstructural and chemical changes which produce these reservoir characteristics and discusses the implications of these processes on reservoir quality and fluid migration in intrusion-rich sedimentary basins.

1. Introduction:

Magmatism within sedimentary basins can lead to local increases in temperature and fluid pressure, and the circulation of hot mineralising fluids through pore and fracture systems (Einsele et al., 1980, Einsele, 1988; Senger et al., 2014, Sydnes et al., 2019). These hot fluids can alter the chemistry of the rock by mobilising and redistributing minerals. Fluid-rock interactions can take place on a local scale around an individual sill over a relatively short time frame, i.e. months to tens of thousands of years (Monreal et al., 2009), or on a regional scale over a longer duration, i.e. millions of years, within a basin affected by magmatic activity (Einsele et al., 1980; Duddy et al., 1994; Coffin & Eldholm, 1992). Such systems can be found worldwide where active rifting and continental breakup occurs (White & Mckenzie, 1989; Holford et al., 2013; Senger et al., 2017). Due to the ability of hydrothermal fluids to concentrate valuable metals much of the previous work on mineralisation around intrusions is focussed on the mining industry and accumulation of economic ores within veins (Taylor, 1974; Grant et al., 1977; Edwards & Atkinson, 1986; Monteiro et al., 2008). With increasing exploration for hydrocarbons in sedimentary basins affected by magmatism, (e.g. the Faroe Shetland Basin, North Atlantic margin (Rateau et al., 2013; Schofield et al., 2015; Muirhead et al., 2017, 2018), Gunnedah and Carnarvon Basin, Australia (Othman et al., 2001; Holford 2013, Rohrman, 2013), Cambay Basin, India (Gupta, 1981; Arora et al., 2017) Paraná, Amazonas and Parnaiba basins, Brazil (Araújo et al., 2000; Thomaz Filho et al., 2008; Rossetti et al., 2019) and Neuquén basin, Argentina (Monreal et al., 2009)) there is a growing need to understand how intrusions and associated hot fluids impact host rocks.

Within petroleum systems, evidence has shown that intrusions can 1) aid source rock maturation by thermally maturing organic material (Simonet et al., 1981, Raymond & Murchinson 1988; Bishop & Abbot, 1995, Galushkin, 1997; Aarnes et al., 2010; Muirhead et al., 2017; 2018) and 2) affect hydrocarbon migration by acting as a barrier or baffle to fluid flow, in addition to acting as potential basin scale migration conduits (Rateau et al., 2013; Schofield et al., 2015). But empirical data quantifying the effects of intrusions on reservoir quality is limited. It is generally perceived that igneous intrusions will locally (100-200 % intrusion thickness) reduce sandstone porosity and permeability as heating and movement of pore fluids alters and dissolves framework minerals and cements are precipitated from solution (Einsele et al., 1980, Einsele, 1988; Kastner & Gieskes, 1981; Senger et al., 2017). Whilst changes to porosity and permeability have been attributed to mineral alteration and due to metamorphism and hydrothermal fluids, few studies provide quantitative measurements of the degree of alteration that occurs. Mckinley et al., (2001) observed mineral and textural changes to the pore filling clays within a sandstone in proximity to a 2 m sill but found little effect on porosity and permeability. Townsend (2018) examined sandstones away from a 2 m dyke

observing reduction in porosity and permeability at the dyke aureole up to 50-70 cm due to recrystallised quartz and precipitation of amorphous iron rich cement. In this study we focus on two sandstones with differing pore filling materials, to understand the reservoir quality and mineralogical changes that may occur through emplacement of igneous intrusions and hydrothermal fluids.

Cementation is one of the most significant factors affecting host rock reservoir quality. This study quantifies changes in the reservoir quality (porosity and permeability, microstructure and geochemistry) of sedimentary host rocks as a function of distance from an igneous intrusion. These results are used to interpret the processes controlling reservoir quality around igneous bodies. The implications whilst useful for hydrocarbon reservoirs within magmatic basins may also be relevant to groundwater storage (Chevallier et al., 2001), anthropogenic CO_2 storage (Senger et al., 2014) and extraction of geothermal energy (Campbell et al., 2016).

2. Geological Context:

The west coast of Scotland records widespread evidence of Palaeogene volcanism during the active rifting and extension of the North Atlantic, known as the North Atlantic Igneous Province (NAIP). This includes lava fields, plutons, sill complexes and dyke swarms (Emeleus & Bell 2005; Schofield et al 2016). Field observations and samples for this study have been taken from two Palaeogene basaltic intrusions (typical of the intrusions encountered in regions such as the West of Shetland (Bell & Butcher 2002; Schofield et al., 2015)); a sill emplaced into calcareous sandstone (sensu Forgotson, 1974) on the northern coast of Ardnamurchan, and a dyke emplaced into clay rich sandstones at Spireslack quarry, East Ayrshire (Fig. 1). Similar intrusions have been dated to c.60-58 Ma (Emeleus & Bell, 2005).

[please insert Figure 1]

2.1. Ardnamurchan- calcareous sandstone

The calcareous sandstone samples were collected from west of Ockle point, Ardnamurchan (Lat: 56.764501, Long: -6.016519). The 2.3 m thick Ardnamurchan sill is a compound dolerite sheet (1.9m and 0.4m sills) in direct contact with a sandstone below (Fig. 2). The sill is hosted by Lower Jurassic (Hettangian-Sinemurian) calcareous sandstones, which make up part of the Breakish Formation. Regionally, these sandstones were deposited in Triassic half grabens of the Hebrides basin and locally filled the Inner Hebrides Basin, West of Scotland (Hesselbo et al., 1998). The Breakish Formation is

interbedded with the offshore equivalent marine muds, marls and limestones also seen in Ardnamurchan representing transgressive-regressive facies cycles (Hesselbo et al., 1998). These outcrops provide analogues to Mesozoic sedimentary rocks offshore west of Scotland and Ireland (Hesselbo & Coe 2000) as well as Lower Jurassic sediments west of Shetland. The studied sedimentary section measures c. 1.5 m in height and comprises fine-medium grained, well cemented, structureless sandstone with calcite veins (Fig. 2).

[please insert Figure 2]

2.2. Spireslack- clay rich sandstone

Spireslack is a Carboniferous open-pit coal mine south of Glasgow, Scotland, UK (Fig. 1) which provides a ~1 km long, ~80 m deep exposure (Leslie et al., 2016). The intrusions cut deposits of the Limestone Coal Formation (LCF) of Visean–Namurian age (330 Ma to 325 Ma). The LCF is typical of Carboniferous strata deposited in the Midland Valley of Scotland containing regionally correlatable marine limestone and mudstones, deltaic fluvial sandstones and terrestrial palaeosol horizons and coal beds. Sandstones throughout the LCF display cross bedding, stacked bars, point bars and are channelised in places (Ellen et al., 2019). The exposed sequence is cut by several Palaeogene basaltic vertical dykes of varying thickness, from a few centimetres to over 3 m. Often the dykes are altered and transformed to pale cream/brown alteration product known as 'white trap' where it intrudes coal or carbonaceous mudstone layers (Mykura, 1965; Ellen et al., 2016). The original dolerite structure is retained but the constituent minerals are pseudomorphed by kaolinite, chlorite, leucoxene, amorphous silica and carbonate (Cameron & Stephenson, 1985). The basaltic dyke studied is 3 m wide and extends vertically 80 m up the quarry wall (Fig. 3). Samples were extracted from a 30 cm thick bed highlighted in yellow (Fig. 3b). This bed/layer was selected as it is continuously exposed along the 10 m sampling transect and had no other intrusions in close proximity to the sampling area.

[please insert Figures 3]

3. Methodology:

The extent of thermal alteration is expressed with respect to intrusion thickness, % i.t. (percentage of intrusion thickness) (Fig. 4). Using percentage of intrusion thicknesses allows comparison of

aureole/alteration extent between dykes and sills of different sizes and orientations. Host rock sandstones were sampled along transects taken perpendicular to the intrusions up to 56 % i.t. at Ardnamurchan for the calcareous sandstone (due to exposure limitations), and 330 % i.t. at Spireslack for the clay rich sandstone which was deemed a sufficient distance to account for thermal aureole affects.

[please insert Figures 4]

3.1. Sample preparation

Samples were prepared by removing weathered sections and coring a total of 109 plugs (34 calcareous sandstone, 75 clay rich sandstone) from blocks collected in the field. These plugs measured 2.56 cm in diameter, and were taken in both vertical and horizontal orientations (with respect to bedding). Plug diameters and lengths were recorded from an average of 10 digital caliper measurements accurate to 0.01 mm. Core lengths ranged from 1.30 - 6.44 cm. Plugs were dried for 24 hours at 40° C to remove remaining water. Cut plug ends were used for thin section preparation for petrographic inspection by optical microscopy, Cold Cathodoluminescence (CL), Scanning Electron Microscopy (SEM) including Energy Dispersive Spectroscopy (EDS).

3.2. Porosity permeability measurements

3.2.1. Porosity measurements

Effective porosity was measured using a helium injection porosimeter, which determines pore volume of plugs based on Boyle's law – which assumes that gas pressures have a positive correlation to gas volumes. Bulk volume is estimated from the mean length and diameter of the plugs measured with callipers. Tests were run at room temperatures, 18 - 20°C. Plugs were placed into a closed chamber and the volume of helium gas that can enter the compartment indicates the effective (connected) porosity of the plug. This was calibrated to a known volume and recalibrated every 0.4^{o}C change in temperature to ensure pressure was not affected by temperature (only by volume).

3.2.2. Mercury injection porosimetry (MIP)

MIP was used for the calcareous sandstone contact (0-6 % i.t.) as the rock was too weak to create a fully intact cylindrical plug. MIP tests were performed with a Micrometrics AutoPore IV 9500. Measurements were conducted in two stages: a manual low pressure run at 0.54 psia, and an automated high pressure run from 0.1 to 60000 psia. After low-pressure testing, the penetrometer

158 was removed and weighed before high pressure testing. The machine was set to equilibrate for 10 s
159 at a contact angle of 143°. MIP method is comparable with plug porosity measurements for
160 sandstones (Debenham et al., 2019).

161 *3.2.3. Permeability measurements*

162 Steady-state permeability was measured using nitrogen gas as the permeant at steady state
163 conditions, flowing along the axial direction of the plugs applying a confining pressure of 2.7 Mpa in
164 a Hassler type core holder. Permeability was calculated using a modified Darcy equation expressed
165 as:

166 $$K = 2\mu Q\left(\frac{L}{A}\right)\left(\frac{Pa}{(P1-P2)^2}\right)$$

167 Where K = permeability (millidarcies, mD), μ = viscosity (centipoise, cP), Q = gas flow rate (calculated
168 from V/t, volume of fluid (cm^3) passed in time (s^{-1}), L and A = plug length and cross-sectional area (cm
169 and cm^2, respectively), P_a = atmospheric pressure, P_1 and P_2 are the input pressure and output pressure
170 respectively (atmospheres). An average gas pressure (P_{mean}) was calculated for each plug from a range
171 of input and output pressures. Klinkenberg correction allows gas permeability measurements to
172 approximate the permeability of a plug with a liquid flowing through it (Klinkenberg, 1941; Tanikawa
173 & Shimamoto, 2009). Uncertainty of variables include mean plug length from 10 calliper
174 measurements accurate to 0.01 mm, Flow rate measured from a stopwatch within human precision
175 of ± 0.2 s, pressure measurement uncertainty to ± 0.1 psi, accuracy of pressure gauges to 0.1 % and
176 viscosity ± 0.2 % (0.00034 cp calculated across a range of room temperatures) (Farrell et al. 2014).

177

178 **3.3. Petrographic and Microstructural analysis**

179 Petrographic analyses were performed on doubly polished thin sections prepared at Aberdeen
180 University. Mineralogy and cements were examined in plane polarised and cross polarised light and
181 imaged using a Nikon SMZ25 stereomicroscope with Nikon DS-Fi2 camera and Nikon Elements
182 software or a Leica DM750P and mounted Leica ICC50 E camera and Lecia LAZ EZ software. Eight thin
183 sections were made from the ends of the calcareous sandstones plugs collected at varying distances
184 from the intrusion (0, 7, 15, 22, 28, 35, 43, 56 % i.t.). Four thin sections were made for clay rich
185 sandstone (0, 27, 47, 330 % i.t.).

186 *3.3.1. Scanning Electron Microscopy & Energy dispersive X-ray spectroscopy*

187 Scanning Electron Microscopy (SEM) analyses were conducted using a Zeiss GeminiSEM 300 VP FEG
188 SEM. Sample sets for both Spireslack and Ardnamurchan were analysed to identify composition of
189 minerals and cements that may not be identifiable by optical microscopy (Huggett, 1984, White et al.,
190 1985). Six calcareous sandstone thin sections were carbon coated and examined using back-scattered
191 electron imaging (BSE). Secondary electron imaging (SE) was performed on seven clay rich sandstone
192 rock fragments for identification and analysis of clay type. Energy dispersive x-ray (EDS) analyses was
193 used to generate semi quantitative false colour maps identifying chemical variations in both sample
194 sets.

195

196 *3.3.2. Cold Cathodoluminescence*

197 Cold Cathodoluminescence (CL) was used to determine separate phases of calcite cement for the
198 calcareous sandstone. The brightness of calcite depends on the ratio of Iron to Manganese (Fe: Mn)
199 within the calcite at time of precipitation (Machel & Burton 1991). In carbonates iron acts as a
200 quencher dimming the brightness and manganese increases the brightness. A range of trace elements
201 known as sensitisers can also affect the ability of Fe and Mn to change brightness allowing CL to be
202 used to identify chemical changes. Thin-sections were examined with a petrographic microscope
203 (Nikon Microphot FX equipped with Nikon DS Fi2 camera and Nikon Elements D software), and optical
204 cold cathode cathodoluminescence (CL) stage (CITL Mk 3) at 15-20 kV with a current of c. 350 µA.

205

206 *3.3.3. X-ray diffraction*

207 Quantification of bulk rock mineralogy and clay fraction was completed using XRD analysis on
208 powdered samples. The sample is first disaggregated gently using a pestle and mortar. A 2g split of
209 this material is then 'micronised' using a McCrone Micronising Mill to obtain an x-ray diffraction
210 'powder' with a mean particle diameter of between 5 - 10 microns. The sample as a slurry is dried and
211 the powder is front-packed into an aluminium cavity mount, producing a randomly orientated sample
212 for presentation to the x-ray beam. XRD was carried out on four of the clay rich sandstone samples at
213 0, 27, 47 and 330 % distance from the 3 m dyke. Samples were chosen to quantify the changes in clays
214 observed from SEM imagery. For clay fraction analysis samples were further separated by ultrasound
215 and centrifugation to obtain <2-micron clay fraction and analysed between 3° and 35° 2Θ (theta) at a
216 step size of 0.05°/sec using x-ray radiation from a copper anode at 40 kV, 40 mA. An indication of the
217 clay minerals crystallinity was given by assessment of the peak width. Clay fraction analysis was

conducted on a Philips PW1730 generator instrument. Siroquant software was used to implement the Rietveld equation and refine the results by comparing outputs with the experimental trace.

4. Results

4.1. Measured reservoir quality

4.1.1. Porosity

Helium porosities measured from 34 plugs of Ardnamurchan calcareous sandstone were plotted relative to their distance to the intrusion (Fig. 5a). Helium porosities ranged between 0.35 and 9.43 % with samples located > 35 %i.t. from the intrusion showing the highest porosities. Contact rock samples adjacent to the intrusion were too fragile to core therefore a mercury injection porosity of 39.84 % was measured (annotated in Fig. 5a). Pore connectivity was relatively high in this sample with mercury saturating the sample up to 95 % by just 1500 psi. Analysis of MIP data measured pore throat sizes between c. 5-55 µm. The high porosity of the contact rock is consistent with a lack of visible cement in hand samples (see Section 4.2.1). Porosities were significantly lower outside of the contact zone (0-6 % i.t) and then increased with distance from the sill, from an average porosity of 1.4 % between 7-35 % i.t. up to an average porosity of 6.4 % between 35-56 % i.t. from the sill (Fig. 5a).

[insert Figure 5 double width]

Helium porosities measured from 75 plugs of Spireslack clay rich sandstone ranged between 5 and 25 % (Fig. 6a). Host rock sampled furthest from the intrusion (330 % i.t.) had an average porosity of 19.9 %. Porosity has a strong decreasing trend from >20 % at the furthest distance from the intrusion down to < 5 % at around 50 % i.t. from the intrusion. Close to the intrusion contact (0-17 % i.t.) porosities were shown to rebound, increasing up to an average porosity of 10.3 % (Fig 6a).

[insert Figure 6 double width]

4.1.2. Permeability

Klinkenberg-corrected permeabilities were measured for calcareous sandstone plugs sampled with increasing distance from the 2.3 m thick sill, from c. 5 to 56 % i.t. Permeabilities ranged over 4 orders of magnitude from 0.0001 to 4.6 mD (Fig 5b). Permeabilities showed an overall decreasing trend with proximity to the sill (Fig. 5b). The highest value of 4.6 mD is likely due to a macro fracture within the plug at 56% i.t.. The fracture is parallel to bedding and not thought to be related to the intrusion and has been excluded from the calculated average in order to assess the mineralogical affects related to the intrusion only. Between 5-32 % i.t. permeabilities averaged 0.002 mD. Samples between 35-56%

i.t. had an average permeability of 0.054 mD. There is a shift in average permeability by one order of magnitude for the samples >35 % i.t.. Permeability was calculated from MIP data for the contact zone (0-6 % i.t.) sample using the Katz-Thompson model (Katz and Thompson 1986) to derive a permeability of 241 mD.

Permeabilities of clay rich sandstone samples also ranged over 4 orders of magnitude between 0.0003 and 7.45 mD (Fig. 6b). For the more distal background samples (150-330 % i.t.) permeabilities averaged at 0.70 mD (n=36). Permeabilities of background host rock samples ranged over 2 orders of magnitude (0.05-2.96 mD) due to anisotropy of permeability induced by sedimentary lamination, with highest permeabilities measured in plugs oriented parallel to lamination and lowest permeabilities in plugs oriented normal to laminations (Fig 6b). From 100 % i.t. permeabilities of all plugs (parallel and normal to lamination) was reduced to <0.1 mD, with lowest permeabilities measured in samples from 47% i.t. (average 0.0066 mD (n=7)). Between 35 % i.t. and 100 % i.t. sedimentary lamination is shown to maintain a control on anisotropy of permeability, however below 35 % i.t. this is less clear. Close to the contact average permeability increased to 0.85 mD (n=12) up to 17 % i.t. from the intrusion. A permeability of 7.45 mD was measured at 27 % i.t.. This high permeability was due to a macro fracture within the plug. Field observations described increased fracturing in the vicinity of the intrusion, so this measurement is thought to be geological and not induced by coring. Some samples in the vicinity of the dyke contact were heavily fractured and un-coreable and therefore permeability is likely to be underestimated for the contact zone.

4.2. Petrography and microstructural properties

4.2.1. Calcareous sandstone

Calcareous sandstone mineralogy is consistent throughout the eight thin-sections examined from 0 to 56 % i.t.. The sandstone is predominantly quartz dominated but also contains feldspar (sodic plagioclase and K-feldspar), carbonate grains and mica. Cements consist of micrite and larger sparry calcite crystals. Quartz and feldspar grains are sub-angular and moderately to well-sorted often displaying irregular grain edges (Fig. 7). Most grain contacts are points with some evidence of convex-concave grain contacts (Fig. 7). Carbonate allochems including shell fragments and peloids were present predominantly within the area 7 to 35 % i.t. Within this zone quartz and feldspar grains were commonly seen ‘floating’ in micritic cement (Fig. 7). The contact between the sandstone and the basaltic intrusion is a brown, undulating zone that measures c. 2 cm to 15 cm (i.e. about 6.5 % i.t.) in thickness (Fig. 2e). In the field this contact zone appears friable and lacks obvious cementation with a

brown colouration. Calcite veins oriented both horizontally and vertically, are most prominent up to 35 cm (15 % i.t.) from the contact zone (Fig. 2c,d).

[Insert figure 7 double spaced]

Calcite is the predominant pore filling cement, observed in optical micrographs (Fig. 7). Energy Dispersive Spectroscopy was used to determine the elemental compositions of grains and cements as shown in false colour maps (Fig. 8). Results showed that the majority of grains were quartz (50-70 %) and feldspar (10-20 %). Carbonate grains, cements and porosity made up the remaining rock volume. Carbonate cements and grains have a similar chemistry, and both were denoted as false dark blue (containing calcium)in EDS maps.

[insert figure 8]

Hand specimens from the contact zone (c. 0-6 % i.t. from intrusion) were noticeably different from the rest of the calcareous sandstone having a rusty brown colour and a lower density, likely due to a lack of carbonate cement (Fig. 7, Fig. 8). In these samples intergranular porosity was visible with the naked eye. Whilst no carbonate cement was identified in the contact zone, a brown opaque cement was observed which coated both pores (Fig. 7) and fractures. Point analysis identified this dark cement to be an iron-rich aluminosilicate with traces of magnesium. Iron-rich cement was only identified within the contact zone.

Further away from the contact zone (between 7 and 35 % i.t.) samples were clogged with carbonate cements and had little visible pore space. These cements were identified as dull brown micrite which surrounded grains and sparry calcite crystals ranging in crystal size from c.50-500 µm which frequently filled intergranular porosity. (Fig. 7). Beyond a distance of 35 % i.t. visible porosity was increased, and the size and volume of carbonate cements was reduced. Micrite was still seen surrounding grains with and sparry calcite crystals generally appeared smaller 50 µm or less. These changes in visible porosity can be observed on EDS maps by an increase in pore area, represented by black space (Fig. 8c). At 45 % i.t. (Fig. 8c) large convex pores of a similar size to framework grains indicate that these pores represent secondary porosity generated by dissolution of framework grains.

Cathodoluminescence (CL) was used to investigate the variation of calcite chemistry and phases of cementation (Fig. 9). Results from these analyses can be used to infer the diagenetic history. Samples from the contact zone do not show any luminescence due to the absence of calcite, matching the transmitted light microscopic analyses . All other samples from 7-56 % i.t. showed carbonate mineralogy of varying luminescence. Three types of calcite were identified: (1) Calcite micrite rim (dull brown CL) coating quartz and feldspar grains, (2) micrite, (bright red CL, dull brown in plane polarised

light (ppl)) surrounding grains, (3) sparry calcite (dull (S2) and bright (S1)) filling intergranular porosity. The bright sparry calcite (S1) occurred between 35-56 % i.t. with lower luminescence and smaller crystal size (>100µm) (Fig. 9b). Between 7-28 % i.t. in close proximity to the dyke duller sparry calcite (S2) was observed generally as larger crystals , (>250 µm) with a low CL luminescence (Fig. 9a).

[insert figure 9]

4.2.2. Clay rich sandstone

The clay rich sandstone mineralogy is predominantly quartz (c.>90 %) with minor components of sodic and potassic feldspars and micas. Quartz and feldspar grains are moderate to well-sorted and sub angular to sub-rounded. Grain size is predominantly very fine to fine grained sand with silt/clay mud drapes and asymmetrical ripples (Fig. 3c). Iron oxides are present primarily within close proximity to the intrusion coating detrital grains, however they are also present within fractures at greater distances and as spherulitic siderite within lenses (Fig. 3c and 10). Grain contacts are mostly point but floating textures occur where fractures and fluids have created space. At the contact (0 % i.t.) chemical compaction grain contacts and irregular edges of quartz grains are present as well as dissolved grains creating secondary porosity which were likely feldspars (Fig. 11b).

[insert figures 10 and 11]

Petrography of clay rich sandstones showed variations in both clay type and clay abundance in rocks sampled at a range of distances from the Spireslack intrusion from 0-330 % i.t.. SEM secondary electron observations and EDS maps (Fig. 12 and 13) show that clays (kaolinite and illite) were largely pore residing thought to be occupying dissolved grains and therefore likely authigenic rather than detrital. The pore space of the background sandstone samples c. 200 to 330 % i.t. is predominantly filled with vermicular kaolinite. From EDS maps kaolinite can be identified from aluminium concentrations (false colour green) whilst, illite is identified from potassium presence (false colour blue) (Fig. 12). With increasing proximity to the intrusion (17 to 100 % i.t.) illite was found to be the predominant pore filling material observed from secondary electron SEM. Also identifiable from EDS maps where potassium rich (false colour blue) content interpreted to be illite was more prevalent and a mix of clays illite and kaolinite were present within pore spaces (Fig. 12b). At the dyke contact pore filling material were predominantly iron oxides represented as red with a lesser degree of kaolinite (green) and illite (blue) present. The illite is largely confined to pores which contain no iron oxide (right of Fig. 12a). The Iron oxide beyond 17 % i.t. was generally not pore filling but occurred as coarse spherulitic siderite residing in lenses parallel to bedding (Fig. 10b,d and Fig. 12b,c).

[please insert figure 12]

Geochemical quantification conducted using X-ray diffraction on the clay fraction reported that clays contents were predominantly kaolinite, illite and mixed illite/smectite (comprising ~70 % illite) (Table.1). Clay volume varied between 4.7 and 10 % in four samples. In the context of distance to the intrusion, although these data do not show an overall trend, large changes in the dominant clay type between the contact zone (kaolinite makes up 76 % of clays), the reduced zone (illite is the dominant clay at ~50-60 %) and the background host rock (kaolinite comprises 77 % of all clays) will likely have a significant influence on fluid flow through pores. Crystallographic analysis of clays showed that as well as changes in quantity, the morphology of clays varied between samples from well-crystallised kaolinite at 330 % i.t. to moderately crystallised at 0 %, 27 %, 47 % i.t. (Table. 1). Illite was found to be poorly crystallised for the contact (0 % i.t.) and background (330% i.t.) sandstone samples and moderately crystallised in the reduced section 27 % and 47 % i.t.. Siderite was identified from XRD in small amounts in contact zone samples (Table. 1), as noted by the pore filling iron oxides observed in optical micrographs (Fig. 10). Clay fraction analyses show a relative increase in quartz content from 1.8% at the background sample to >7% in proximity to the intrusion (Table. 1).

[please insert table 1]

Secondary electron detection was carried out on the rough surfaces of clay rich sandstone samples (330, 200 ,100 ,47 ,27 ,7 ,0 % i.t) to investigate the distribution of clays within the pore network (Fig. 13). Identification of clay type was based on morphology and point analysis. Images from this analysis showed increasing occlusion of pores. The background sandstone (330-200 % i.t) displayed large irregular shaped pores containing well-formed authigenic kaolinite booklets and vermicular aggregates located on the edge of pores (Fig. 13a and b). From 100 % i.t. similar size pores were predominantly filled with illite observed growing normal to grain edges and into pore spaces at 47 % i.t (Fig. 13c and d) and well-formed platy aggregates of illite extensively coating grains and filling pores at 27 % i.t (Fig. 13e and f). At the intrusion contact (0-6 % i.t.) some larger pores were visible, partially occluded by a fine grained, rugged mass of very fine kaolinite particles and nodular siderite (Fig. 13g). High magnification images of these pore filling minerals showed smaller kaolinite crystals appear well-formed in comparison to the 'ghost' kaolinite vermiform structure that now contains mostly illite, observed in the lower right hand-side of the micrograph (Fig. 13h).

[please insert figure 13]

6. Discussion

It is typically assumed, (but rarely evidenced empirically) that intruded host rocks (e.g. sandstone or shale) will experience physical-chemical alterations leading to microstructural changes and therefore changes to the reservoir quality properties of host rocks with proximity to igneous intrusions (Taylor, 1974; Reeckman et al., 1985; Einsele, 1988; Esposito and Whitney, 1995). The few studies that have measured porosity and permeability from field samples have reported a reduction in porosity and permeability within the intrusion aureole (Townsend, 2018) whilst other studies report mineral and textural changes but little effect on porosity or permeability (Mckinley et al., 2001). Studies incorporating fluid flow simulations have modelled thermochemical processes in which dissolution and precipitation of silica around intrusions predicts both increases and decreases in permeability (Dutrow et al., 2001; Scott & Driesner 2018).

One of the main adverse effects on reservoir quality is cementation of pore space, with the most common pore filling cement types being calcite, quartz and authigenic clays. This study provides a detailed quantification of changes in cementation, rock microstructure and reservoir quality of Carboniferous deltaic clay rich sandstones from Spireslack quarry and Jurassic marine calcareous sandstones from Ardnamurchan in the framework of distance to a dyke and a sill, respectively. Results from this paper provide much needed information on how the porosity and permeability of common reservoir sandstones may be impacted by nearby igneous intrusions.

6.1. Alteration of host rock cements

Mineralogy of cements and clays were found to vary with distance from the intrusions in both sites. Of particular note is that both intrusions showed a significant reduction in cement/clay at the contact zone leading to an enhanced porosity and permeability zone.

At both contacts iron-rich cements were observed coating grains and filling fractures up to 6 % i.t for the calcareous sandstone and 27 % i.t. for the clay rich sandstone. Magmatic fluids are often rich in metals: in both sample sets we see evidence of metal-rich fluids interacting with the host rock and filling porosity left by dissolved cements. The presence of iron oxide likely indicates the minimal extent of hydrothermal and magmatic fluids into the host rock. Occurrences of iron-rich material at the contact zone between intrusion and sedimentary host rock have also been noted in other porosity-permeability studies relating to intrusions (Townsend, 2018).

408

409 *6.1.1. Calcareous sandstone*

410 For the calcareous sandstone, calcite cement was not present within the contact zone (0-6 % i.t.)
411 adjacent to the intrusion (Fig. 7). Acidic waters associated with igneous intrusions have been
412 documented to aid in carbonate dissolution and generation of secondary porosity (Parker, 1974,
413 Einsele, 1988). Carbonates experience retrograde solubility whereby solubility of calcite falls with
414 increasing temperature (Giles & Boer, 1989) therefore the initial heating from intrusions would
415 decrease solubility. However, cooling of hydrothermal fluids post intrusion would have the ability to
416 dissolve calcite. The most common volatiles released during crystallisation of magmas are
417 predominantly H_2O and CO_2 (Podladchikov & Wickham, 1994). CO_2 rich waters would aid in lowering
418 pH, increasing the likelihood of calcite dissolution. Evidence of calcite precipitation was noted from
419 calcite filled veins which were most frequent in the 7-18 % i.t. interval (Fig. 2) suggesting that the
420 majority of calcite precipitation occurred in close proximity to the intrusion. Esposito and Whitney
421 (1995) noted a replacement of carbonate grains and an increase of authigenic carbonate near thin
422 intrusions in Southwestern Washington, finding carbonate to decrease sharply at the contact for
423 sandstones with minor and varied carbonate content.

424 Dissolution and precipitation of $CaCO_3$ depends on temperature, alkalinity, pH and other factors.
425 When waters of different chemistries mix, changes to the ionic strength can lead to supersaturation
426 or under-saturation with respect to carbonate leading to precipitation or dissolution, respectively
427 (Singurindy & Berkowitz, 2004). Fluid mixing has been shown to be an important process for creating
428 significant porosity within carbonate rocks (Corbella et al., 2006, 2003). Magmatic activities can
429 provide hydrothermal fluids and lead to fluid convection if the porosity and permeability are high
430 enough (Wilson et al., 2007). The calcareous sandstone was sampled from below the sill. Due to the
431 impermeable nature of igneous rocks it is possible that hot fluids would be constrained, potentially,
432 for a longer duration in comparison to overlying strata, which may be an important factor in the
433 mineralisation process which led to the removal carbonates at the contact. We suggest that the
434 contact zone which has experienced significant enhanced porosity represents the dissolution front
435 where magmatic waters and formation waters interact. We infer the sill host rock contact represents
436 the initial rock mixing zone where pore fluids have become under-saturated with respect to carbonate,
437 leading to leaching and removal of calcite grains and cement. Dissolution and mobilization of
438 carbonate has led to solution-enhanced porosities of 39.8 % within the contact zone. The carbonate
439 removed from the contact zone may explain the heavily cemented zone between 7-35 % i.t. with an
440 average porosity of 1.4 % also noted by the significant increase in calcite cement seen in thin section

and EDS maps. It is reasonable to suggest that the increased cement and reduced porosities seen within this zone could be sourced from dissolution and reprecipitation of calcite locally (Fig. 14).

The estimates provided in figure 14 provide a simple mass balance calculation using the measured porosities and distance from the intrusion to calculate the porosity change that might be expected. An initial starting porosity of 6.4 % was based on the background sample assuming this was unaltered by the intrusion. The removed volume of cement required to increase the contact zone porosity was deducted from the volume of initial porosity in the reduced zone. Although basic, the estimates provided in figure 14 show that the volume of carbonate cement removed at the contact zone (if reprecipitated directly below) would reduce porosity from 6.4 % to a calculated 1.2 % which is consistent with the average plug porosity measured within the reduced zone of 1.4 %. This indicates that the dissolved zone could provide a sufficient carbonate source to explain the reduced porosity zone measured from plugs. Furthermore, this suggests that mobilisation of minerals around intrusions can be constrained locally.

[Insert figure 14]

Cathodoluminescence (CL) was necessary to understand the history and identify possible variation in calcite cement types and phases. Whilst CL should not be used to imply environment of deposition (Machel, 1985) it does prove a useful tool in highlighting subtle changes in carbonate chemistry. Iron acts as a quencher dimming the brightness, whilst manganese tends to increase the brightness. A range of trace elements known as sensitisers can also affect the ability of Fe and Mn to change brightness and so different diagenetic events will lead to a difference in observable brightness. Emplacement of igneous intrusions introduce hydrothermal fluids representing a change in fluids and chemistry and therefore present the possibility to have affected cement phases.

From cathodoluminescence examination three types of calcite were identified: (1) calcite rim, (2) micrite and (3) pore filling sparry calcite (Fig. 9) Rims have low luminescence which may suggest original deposition in oxic environments. The micrite cementation is likely to be early (syn-sedimentary) because it is voluminous and exhibits a 'floating grain texture' reminiscent of that seen in calcretes (Wright and Tucker, 1991). There appear to be two phases of sparry calcite with larger dull luminescing crystals in proximity to the intrusion and smaller bright luminescing crystals beyond 28 % i.t.. Close to the intrusion, the lower luminescence of the sparry calcite could have been caused by an increase in iron content or a decrease in manganese (Machel, 1985). Given that iron oxideswere precipitated within the contact zone it is likely that magmatic volatiles were enriched in iron and provide a potential explanation for the change in luminescence (Fig. 9). We infer that this pore filling

473 sparry calcite phase represents the precipitated cement related to hydrothermal fluids within the
474 reduced porosity zone.

475 Optical mineralogy and EDS maps were consistent with porosity data showing a zone of decreased
476 cementation (contact zone) and directly adjacent, increased calcite cement (reduced zone), inferred
477 to have been caused by remineralization and precipitation of the same carbonate volume. The
478 redistribution of calcite cements is believed to have been caused by the mixing of magmatic
479 hydrothermal fluids and pore fluids creating an environment of carbonate under-saturation and
480 removal of cements in proximity to the intrusion.

481

482 *6.1.2. Clay rich sandstone*

483 Thermochemical reactions are known to lead to evolution in clay types and morphologies. With
484 increasing temperature, pH and potassium/water ratio, kaolin and smectite minerals are replaced by
485 illite (Berger et al., 1997; Lanson et al., 2002). Illitisation of illite/smectite layers occur as a progressive
486 transition of enrichment in illite. Kaolinite transforms directly to pure end-member illite at the
487 expense of kaolinite dissolution (Berger et al., 1997). Illitisation often coincides with tectonic events
488 where increased temperature, fluid flow, faulting and fracturing occur (Lanson et al., 2002). The
489 emplacement of igneous intrusions induce significant increase in temperature, fluid flow and altered
490 chemistries presenting opportunities for mineral alteration of clays within the intruded host rocks.
491 Illite can reduce permeability by several orders of magnitude (Macchi, 1987; Pevear, 1999; Wilkinson
492 et al., 2014) and therefore it is important to understand its formation with regards to igneous
493 intrusions and host-rock reservoir quality.

494 Illitisation of mixed illite-smectite has been observed in the vicinity of igneous bodies (Pytte and
495 Reynolds, 1989; Buhmann, 1992; Esposito and Whitney 1995) and hydrothermal fluid migration (Inoue
496 and Utada 1983; Inoue et al., 1992; Sachsenhofer et al., 1998). In these studies, the percentage of illite
497 in mixed illite-smectite clays was found to increase with proximity to intrusions due to thermal
498 alteration. Esposito and Whitney (1995) found illitisation to occur up to 100 % i.t. and Pytte and
499 Reynolds (1989) observed thermal effects on illite-smectite up to 200 % i.t..

500 Illite replacement of kaolinite is a widely observed process in deeply buried sandstones (e.g., Kisch,
501 1979; Chermak & Rimstidt 1990; Ehrenberg et al., 1993; Lanson et al., 1996, 2002). Precipitation of
502 illite is strongly temperature dependent (e.g., Eslinger and Glasmann, 1993; Huang *et al.*, 1993)
503 generally requiring temperatures ~130^{o} C and the presence of potassium rich fluids (Ehrenberg &
504 Nadeau, 1989; Lanson et al., 2002; Bjørlykke, 2010) but may also occur at lower temperatures >60 ^{o}C

505 during enhanced fluid movements and increased volumes of CO_2 (Almon, 1981; Gaupp et al., 1993;
506 Platt, 1993). Most likely sources of potassium for the clay rich sandstone include dissolution of primary
507 potassium feldspars and detrital clays.

508 Illitisation is identified as the predominant factor affecting the reservoir quality of the clay rich
509 sandstone. A change in clay type was observed from SEM observations and XRD measurements (Table.
510 1). Predominantly kaolinite booklets observed in the distal samples (200-330 % i.t.) appeared
511 progressively deteriorated towards the intrusion, with increasing amounts of pore filling illite seen
512 (Fig. 13). At the contact however, clay proportions return to unaltered levels seen at the background
513 with kaolinite dominant and a reduced amount of illite.

514 Illitisation was likely enhanced by the presence of weakly acidic (CO_2 rich) fluids (Thompson et al.,
515 1996) which would be associated with emplacement of the dyke and maturation of organic matter
516 from intercalated coal layers. For acid species to be able to leave organic material it must overcome
517 the buffering effects of hydrosable minerals e.g feldspar dissolution within shales. In the case of coal
518 the organic fraction is usually large enough to overcome the neutralising effects and organic acids can
519 migrate (Berger et al., 1997). Aarnes et al., 2010 modelled intrusion related maturation of organic
520 matter and it is likely that CO_2 will be related to both magmatic and organic derived sources. The
521 availability of CO_2 is assumed sufficient to promote an acidic front which would cause dissolution of K-
522 feldspars and movement of K-rich fluids. Combined with an increasing temperature profile towards
523 the dyke contact the reaction of K-feldspar + kaolinite → illite + quartz + H_2O (at temperatures greater
524 than 120 ^oC) is reasonable.

525 SEM secondary electron (SE) observations found background samples (200-330% i.t.) to contain high
526 proportions of pore filling kaolinite vermiforms. XRD measurements (Table.1) report kaolinite
527 contents of almost 80% for the most distal sample (330 % i.t.). Between (27-100 % i.t.) pore filling illite
528 was more frequently seen filling pores (Fig. 13c-f). XRD whole rock and clay fraction analysis report
529 kaolinite content to be depleted at 27 and 47 % i.t. and illite to be comparatively higher than in the
530 distal sample at 330 % i.t.. Morphologies of illite found within pore spaces comprised of well-formed
531 platey aggregates which represent end member illite with moderate crystallinity (Table. 1). The
532 delicate curved plates (Fig. 13f) are clearly authigenic with crystal structure unlikely to have been
533 preserved through transportation. In addition to increasing illite content within pores, illite was also
534 found within vermiforms as pseudomorphs after kaolinite (Fig. 13h). This suggests that illite replaced
535 k-feldspar and authigenic kaolinite in pores as well as kaolinite vermiforms. Secondary porosity seen
536 in optical microscopy (Fig. 11) and SE (Fig. 13a) is thought to have been generated from K-feldspar
537 dissolution as mentioned above. Kaolinite is assumed to have replaced K-feldspar away from the

intrusion and latterly replaced by illite where temperature and k-rich fluids where available i.e. in vicinity to the intrusion.

Evidence of increasing illite content support the measured reductions in porosity and permeability within the 17-200 % i.t zone (Fig.6). The zone of maximum illitisation occurs around 50 % i.t. corresponding directly with the lowest permeability average of 0.007 mD compared to the unaltered sandstone average of 0.81 mD, a reduction of three orders of magnitude.

Illitisation in the vicinity to the intrusion is likely to be the primary cause of permeability decrease due to elevated host rock temperatures. However, heterogeneities seen from hand specimens e.g (Fig. 2e) including siderite lenses and mud drapes provide possibilities for clay variation in measurements. Whilst siderite lenses were found within samples selected for thin section preparation and correspondingly EDS maps mud drapes were not and so cannot be assessed. Fine iron oxides which coated pores and filled fractures at the contact are assumed to be related to the intrusion. The spherulitic siderite containing coarse crystals found in lenses parallel to bedding is often associated with soil formation and most likely formed during early diagenesis.

The increase in porosity and permeability at the contact (0-17 % i.t.) coincides with a decrease in illite, increase in kaolinite and presence of fine iron oxides coating pores. EDS maps (Fig. 12) highlight chemical concentrations of sample sandstones and can be used to assess chemistry and therefore clay type within intergranular porosity. The contact sample (Fig. 12a) shows a lack of potassium (false colour blue) indicating less illite/mica at the contact compared with the adjacent 27 % i.t. sample where both illite and kaolinite are interpreted from potassium (blue) and aluminium (green) concentrations within intergranular porosity. This suggests illite crystallisation either didn't occur to the same extent at the contact or was removed.

The observed decrease in illite may be due to: (1) Thermal destruction of illite at the contact by increased temperature. Temperatures at the contact between dyke and host rock would be in the range of 500-700 ^{o} C (Delaney, 1987). Illite has a temperature stability range from c. 200-300^{o} C, above 300^{o} C muscovite is produced (Thompson et al., 1996). Low volumes (5%) of illite and mica measured from XRD (Table.1) at the contact may indicate that potassium rich fluids were driven away from contact due to high temperatures and fluid pressures. (2) Conversely the presence of iron at the contact (Fig. 12) may have mechanically restricted K-rich fluids and restricted the illitisation reaction. With either reactive grains being protected from dissolution or alteration or prohibiting illite nucleation. Esposito & Whitney, (1995) suggested magnesium, iron and calcium mobilised from mafic rocks could saturate sediments inhibiting the illitisation reaction. Magnesium present within the iron oxides may also aid in retarding the illitisation reaction (Huang et al., 1993). A combination of both

these mechanisms seems likely with iron filling many of the pore spaces and larger aggregates of illite/muscovite at the contact appearing restricted to areas with less iron (Fig. 12a).

Increase in proportion of kaolinite at the contact may have also been sourced from the adjacent dyke which is heavily altered to white trap providing a source for both kaolin and iron. Given the higher porosities at contact compared to the illitised zone later fluid movements could conceivably restrict fluid flow along dyke contact. Kaolinite at the contact appears as smaller well-formed crystals (Fig. 13h) compared to deteriorated larger vermiforms and may present a later stage of kaolinite precipitation.

6.2 Extent of reservoir quality alteration

From reservoir quality transects (porosity and permeability) for both calcareous and clay rich sandstone, three broad zones have been identified: (1) The contact zone adjacent to the intrusion which in both cases was found to have enhanced reservoir quality, (2) The reduced zone which shows a decrease in both porosity and permeability with proximity to the intrusion, and (3) the unaltered zone where reservoir quality plateaus and is assumed to have been unaffected by the intrusion previously described as background zone/sample.

For the calcareous sandstone the contact zone in which reservoir quality increased occurred up to 15 cm from the 2.3 m dyke (c. 0-6 % i.t.). The reduced zone 7-35 % i.t. from the intrusion had a decrease in plug porosity and permeability and a visible increase in cement volume (Fig. 7), attributed to mineralisation associated with the emplacement, heating and cooling of igneous intrusions and their attendant hydrothermal fluids. Within this zone porosity showed a relative reduction of around 5 % from unaltered samples which increased to an absolute porosity of 38 % directly adjacent to the intrusion within the contact zone. The assumed unaltered sandstone (35-56 % i.t.) average porosity of 6.4 % may continue to increase but due to the limitations of exposure to 56 % i.t. the change of properties further away could not be measured. Permeability follows a similar trend to porosity with a reduction of one order of magnitude from c. 0.05 mD to 0.0015 mD between unaltered and reduced zones. From reservoir quality changes we have determined the thermal aureole (distance of thermal effect) of the 2.3 m thick dolerite sill to extend 35 % i.t. within the calcareous sandstone. Within this area sandstone quality is both positively (0-6 % i.t.) and negatively (7-35 % i.t.) affected.

The (re)distribution of the carbonate cements could be due to three diagenetic factors: reactions occurring pre, syn or post-intrusion. Firstly, pre-intrusion: where depositional variation in the dominant control. Optical micrographs (Fig. 7) show more carbonate grains within the cemented zone

603 which would provide a likely source for the increase in cements seen. The absence of carbonate
604 material from the contact is more difficult to explain based on depositional variation and likely due to
605 other factors. The original pore filling material of the contact zone is unknown; however, it can be
606 presumed to be carbonate cements as this is the only cement throughout rest of the strata studied.
607 Secondly, syn-intrusion: carbonate distribution may have been affected by emplacement of magma
608 and hydrothermal fluids dissolving cements at the contact which could represent a potential source
609 for large sparry calcite seen within the cemented zone. Thirdly, post-intrusion, absence of cement at
610 the contact could have occurred due to fluid movement being constrained beneath an impermeable
611 sill leading to enhanced fluid movement and removal of cements over a longer geological duration.
612 This may include weathering near surface however, it is thought that such extensive removal of calcite
613 would not have been limited to the thin contact zone as seen in this study.

614 We cannot rule out entirely the diagenetic mineralisation due to variations in grain size, original
615 composition and depositional environment. The reduced zone which is the more cemented unit
616 contains more carbonate grains and may partially be due to depositional environment. However, the
617 data presented in this study are consistent with this being further enhanced by hot fluids and
618 mineralisation associated with the intrusion. Given the significant loss of carbonate cement at the
619 contact which cannot be explained purely by depositional and grain size variations, we interpret this
620 loss of carbonate to be a viable source for the increase in sparry calcite within the reduced zone.

621

622 The clay rich sandstone was sampled to a distance of 10 m (c. 330 % i.t.) from the 3 m dyke. Porosity
623 was reduced within the interval of 17-200 % i.t. and permeability reduced within 27-150 % i.t..
624 Increasing illitisation with proximity towards the Spireslack dyke is attributed as the main factor in
625 contributing to the observed reduction in porosity. An average unaltered porosity of 20 % is lowered
626 to an average 6 % within the reduced zone, followed by an increase up to 10 % porosity average at
627 the intrusion contact (0-17 % i.t.). Similarly, permeability decreases to an average of 0.006 mD within
628 the defined reduction zone (27-150 % i.t.) but increases by 2 orders of magnitude within the contact
629 zone (0-27 % i.t.) matching and surpassing unaltered host rock measurements. Interestingly
630 Smallwood & Harding et al., (2009) also noted a differing effect between porosity and permeability
631 measured from well data in the Faroe-Shetland basin, in both cases this is likely due to the relationship
632 between precipitating minerals and reservoir quality with illite having a much larger effect on
633 permeability. For the clay rich sandstone, the aureole of effected reservoir quality is observed up to
634 150-200 % away from the 3 m Spireslack dyke.

The variation in reservoir quality from enhanced contact zone to the reduced zone in both cases (calcareous and clay rich sandstones) is interpreted to be a consequence of the alteration due to hydrothermal fluids. It should be noted that for both studies fracture intensity increased toward the intrusion which is unrepresented within the plugs cored and therefore permeability is likely underestimated at the contact zone. These fractures related to cooling of the intrusion would likely increase fluid flow within the intrusion and host rock and have been suggested as potential migration pathways (Rateau et al., 2013; Senger et al., 2014).

6.3 Implications for igneous intrusion induced alteration of reservoir quality

For both intrusions, convection of hydrothermal fluids and elevated temperatures are thought to be the driving factors for mineral alteration, with both dissolution and precipitation leading to removal/addition of pre-existing clays and cements producing the enhanced reservoir quality observed at host rock-intrusion contact zone. This enhanced zone was found up to 5 % i.t. for Ardnamurchan sill and 17 % i.t. for the Spireslack dyke.

As mentioned in previous intrusion related studies (Duddy et al., 1984, Einsele et al., 1980, Townsend, 2018) host rocks commonly experience a reduction of reservoir quality with proximity to intrusions. The measured reservoir quality findings described here give quantitative evidence for the magnitude and extent of reservoir quality away from two intrusive igneous bodies for both calcareous and clay rich pore-filled sandstones.

While both intruded sandstones have shown reduced and increased reservoir quality the magnitude of change within the enhanced porosity zone seen in the calcareous sandstone is significant, with an increase in porosity of over 30 % across the contact zone (c. 0-5 % i.t.). For the clay rich sandstone porosity increased within the contact zone (c. 0-17 % i.t.) interval by 5 % and an increase in permeability by three orders of magnitude. It is important to note that porosity for the clay rich sandstone, although higher than the reduced zone was still below that measured from the sample of 20 % porosity at 330 % i.t..

The significant dissolution of calcite at Ardnamurchan may be specific to the intrusion studied and further analyses of host rock interactions from intrusions are required to confirm if this is a common feature. In both sandstones secondary porosity is created by removal of pore filling material due to dissolution and precipitating minerals away from the intrusion. The zones of increased cementation and the cement free contact zone observed from optical and SEM analysis correlate with quantitative measurements of porosity and permeability.

It is not necessarily appropriate to hold to the general assumption that reservoir quality decreases towards igneous bodies. As clearly noted above there are several factors relating to host rock alteration, with mineralisation and porosity-permeability showing an intricate relationship. Both instances of enhanced reservoir quality of interest for understanding fluid flow around intruded sandstones.

We have shown that intrusions have a negative impact on reservoir properties, however these two sample suites demonstrate that intrusion-host rock interactions can lead to significant positive effects on a local scale due to the mineralising effects of hydrothermal and/or magmatic fluids (Fig. 15). The elevated temperatures and pressures associated with emplacement of igneous intrusions and related hydrothermal fluids were found to effect grain and cement dissolution. The highly porous zone (c. 5 % i.t.) found within the calcareous sandstones has the potential to act as an important migration pathway for fluids (water, oil and/or gas) which may have otherwise been impeded in low permeability sandstones and this should be considered when modelling fluid movement and migration. The alteration within thermal aureoles due to conduction heating of organic matter generally impacts around 100 % intrusion thickness with a range of 30-200 % i.t. (Aarnes et al., 2010). Further work is required to address the extent and scalability of these reactions within permeable sediments such as those described here.

[Insert figure 15]

7. Conclusions

From our analyses of two intruded sandstones, reservoir quality was found to be altered both positively and negatively by (1) remobilisation of carbonate cements within a calcareous sandstone and (2) illitisation of pre-existing kaolinite clays within a clay rich sandstone. This study has shown that intruded sedimentary rocks can exhibit a wide range of reactions and the effects on reservoir quality need to be studied on a case-by-case basis. Current assumptions of the negative effect of host rock properties away from igneous intrusions can lead to misinterpretation and therefore the properties of both the intrusion and the host rock mineralogy need to be understood in order to assess migration in the vicinity of intrusions.

Our key findings are:

- Field and laboratory analyses of sedimentary host rock samples from within intrusion aureoles has shown reservoir properties to be both negatively and positively affected.
- Identification of a highly porous zone in the first 5-17 % of intrusion thickness within the host rock indicative of a potential fluid migration pathway.
- Thermal and hydrothermal alteration can have significant impacts on host rock properties, understanding mineralogical changes within thermal aureoles will lead to better models for understanding reservoir quality around igneous intrusions.

This preliminary study provides data on two intrusions intruding two unique sandstones of differing compositions and adds to the growing number of studies on in-situ rocks. Further data and analyses should be conducted in order to assist with models and predictions of the extent and changes expected within igneous aureoles and sedimentary basins affected by magmatism.

Acknowledgements

We thank the reviewers and editor for their helpful comments which greatly improved this manuscript. Thanks to John Still from the University of Aberdeen (ACEMAC) for guidance with SEM/EDS, Colin Taylor for MICP tests and Walter Ritchie for making thin sections. Lorenza Sardisco and Jonathan Wilkins at X-Ray Minerals for XRD analysis and Prof. M.J. Wilson from the James Hutton

727 Institute for valuable discussion of XRD results. Dave Healy acknowledges the support of the Natural
728 Environment Research Council (NERC, UK) through the award NE/N003063/1 'Quantifying the
729 Anisotropy of Permeability in Stressed Rock'.

730 **References:**

731 Aarnes, I., Svensen, H., Connolly, J.A.D. & Podladchikov, Y.Y. 2010: How contact metamorphism can
732 trigger global climate changes: Modeling gas generation around igneous sills in sedimentary basins.
733 Geochimica et Cosmochimica Acta 74, 7179–7195.

734 Almon, W.R., 1981. Depositional environment and diagenesis of Permian Rotliegendes sandstones in
735 the Dutch sector of the southern North Sea. In Clays and the Resource Geologist (Vol. 7, pp. 119-147).
736 Min. Ass. Canada Short Course.

737 Araújo, L.M., Triguis, J.A., Cerqueira, J.R. and Freitas, L.D.S., 2000. AAPG Memoir 73, Chapter 26: The
738 Atypical Permian Petroleum System of the Parana Basin, Brazil.

739 Arora, A., Dutta, S., Gogoi, B. and Banerjee, S., 2017. The effects of igneous dike intrusion on organic
740 geochemistry of black shale and its implications: Late Jurassic Jhuran Formation, India. *International*
741 *Journal of Coal Geology*, *178*, pp.84-99.

742 Bell, B.R., Butcher, H., 2002. On the emplacement of sill complexes: evidence from the Faroe-Shetland
743 Basin. In: In: Jolly, D.W., Bell, B. (Eds.), The North Atlantic Igneous Province: Stratigraphy, Tectonic,
744 Volcanic and Magmatic Processes, vol. 197. Geol. Soc. London. Spec. Publ., pp. 307–329.

745 Berger, G., Lacharpagne, J.C., Velde, B., Beaufort, D. and Lanson, B., 1997. Kinetic constraints on
746 illitization reactions and the effects of organic diagenesis in sandstone/shale sequences. Applied
747 Geochemistry, 12(1), pp.23-35.

748 Bishop A.N. and Abbott G.D. 1995. Vitrinite reflectance and molecular geochemistry of Jurassic
749 sediments: the influence of heating by Tertiary dykes (northwest Scotland). *Organic Geochemistry* 22:
750 165-177.

751 Bjørlykke, K., 2010. Petroleum geoscience: From sedimentary environments to rock physics. Springer
752 Science & Business Media.

753 Buhmann, C., 1992, Smectite-to-illite conversion in a geothermally and lithologically complex Permian
754 sedimentary sequence: Clays and Clay Minerals, v. 40, p. 53-64.

755 Cameron, I B, and Stephenson, D. 1985. British regional geology: The Midland Valley of Scotland. Third
756 edition. Reprint 2014. Keyworth, Nottingham: British Geological Survey.

Campbell, S.A., Lenhardt, N., Dippenaar, M.A. and Götz, A.E., 2016. Geothermal energy from the Main Karoo Basin (South Africa): an outcrop analogue study of Permian sandstone reservoir formations. *Energy Procedia*, *97*, pp.186-193.

Chermak, J.A. and Rimstidt, J.D., 1990. The hydrothermal transformation rate of kaolinite to muscovite/illite. Geochimica et Cosmochimica Acta, 54(11), pp.2979-2990.

Chevallier, L.P., Goedhart, M.L. and Woodford, A.C., 2001. *Influence of Dolerite Sill and Ring Complexes on the Occurrence of Groundwater in Karoo Fractured Aquifers: A Morpho-tectonic Approach: Report to the Water Research Commission*. Water Research Commission

Coffin, M.F. and Eldholm, O., 1992. Volcanism and continental break-up: a global compilation of large igneous provinces. Geological Society, London, Special Publications, 68(1), pp.17-30.

Corbella, M., Ayora, C. and Cardellach, E., 2003. Dissolution of deep carbonate rocks by fluid mixing: a discussion based on reactive transport modeling. Journal of Geochemical Exploration, 78, pp.211-214.

Corbella, M., Ayora, C., Cardellach, E. and Soler, A., 2006. Reactive transport modeling and hydrothermal karst genesis: The example of the Rocabruna barite deposit (Eastern Pyrenees). Chemical Geology, 233(1-2), pp.113-125.

Debenham, N., Farrell, N.J., Holford, S.P., King, R.C. and Healy, D., 2019. Spatial distribution of micrometre-scale porosity and permeability across the damage zone of a reverse-reactivated normal fault in a tight sandstone: Insights from the Otway Basin, SE Australia. Basin Research, 31(3), pp.640-658.

Delaney, P.T., 1987. Heat transfer theory applied to mafic dyke intrusions. Mafic Dyke Swarms, Geol. Assoc. Canada, Spec. Pap, 34, p.31.

Duddy, I.R., Green, P.F., Bray, R.J. and Hegarty, K.A., 1994. Recognition of the thermal effects of fluid flow in sedimentary basins. Geological Society, London, Special Publications, 78(1), pp.325-345.

Dutrow, B.L., Travis, B.J., Gable, C.W. and Henry, D.J., 2001. Coupled heat and silica transport associated with dike intrusion into sedimentary rock: Effects on isotherm location and permeability evolution. Geochimica et Cosmochimica Acta, 65(21), pp.3749-3767.

Edwards, R. and Atkinson, K., 1986. Hydrothermal vein deposits. In *Ore Deposit Geology and its influence on mineral exploration* (pp. 143-174). Springer, Dordrecht.

Ehrenberg, S.N. and Nadeau, P.H., 1989. Formation of diagenetic illite in sandstones of the Garn Formation, Haltenbanken area, mid-Norwegian continental shelf. Clay Minerals, 24(2), pp.233-253.

787 Ehrenberg, S.N., 1993. Preservation of anomalously high porosity in deeply buried sandstones by
788 grain-coating chlorite: examples from the Norwegian continental shelf. AAPG Bulletin, 77(7), pp.1260-
789 1286.

790 Einsele, G., Gieskes, J.M., Curray, J., Moore, D.M., Aguayo, E., Aubry, M.P., Fornari, D., Guerrero, J.,
791 Kastner, M., Kelts, K. and Lyle, M., 1980. Intrusion of basaltic sills into highly porous sediments, and
792 resulting hydrothermal activity. Nature, 283(5746), pp.441-445.

793 Einsele, G., 1988, Mechanism of sill intrusion into soft sediment and expulsion of pore water, Deep
794 Sea Drilling Project, Initial Reports, 64, 1169–1176.

795 Ellen, R., Callaghan, E., Leslie, A.G. and Browne, M.A.E., 2016. The rocks of Spireslack surface coal mine
796 and its subsurface data: an introduction. British Geological Survey, 28pp. (OR/16/053)

797 Ellen, R., Browne, M.A.E., Mitten, A.J., Clarke, S.M., Leslie, A.G. and Callaghan, E., 2019.
798 Sedimentology, architecture and depositional setting of the fluvial Spireslack Sandstone of the
799 Midland Valley, Scotland: insights from the Spireslack surface coal mine. Geological Society, London,
800 Special Publications, 488, pp.SP488-2.

801 Emeleus, C. H. & Bell, B. R. 2005. British Regional Geology: the Palaeogene Volcanic Districts of
802 Scotland, 4th ed.

803 Eslinger, E. and Glasmann, J.R., 1993. Geothermometry and geochronology using clay minerals—an
804 introduction. Clays and Clay minerals, 41(2), pp.117-118.

805 Esposito, K.J. and Whitney, G., 1995. Thermal effects of thin igneous intrusions on diagenetic reactions
806 in a Tertiary basin of southwestern Washington (No. 2085). US Government Printing Office.

807 Farrell, N.J.C., Healy, D., Taylor, C.W., 2014. Anisotropy of permeability in faulted porous sandstones.
808 J. Struct. Geol. 63, 50–67.

809 Forgotson Sr, J.M., 1974. Calcitic Sandstone: GEOLOGIC NOTES. AAPG Bulletin, 58(9), pp.1838-1838

810 Galushkin, Y.I., 1997. The thermal effect of igneous intrusive bodies on maturity of organic matter – a
811 possible mechanism of intrusion formation. Organic Geochemistry 27, 645–658.

812 Gaupp, R., Matter, A., Platt, J., Ramseyer, K. and Walzebuck, J., 1993. Diagenesis and fluid evolution
813 of deeply buried Permian (Rotliegende) gas reservoirs, northwest Germany. AAPG Bulletin, 77(7),
814 pp.1111-1128.

Giles, M.R. and De Boer, R.B., 1989. Secondary porosity: creation of enhanced porosities in the subsurface from the dissolution of carbonate cements as a result of cooling formation waters. Marine and Petroleum Geology, 6(3), pp.261-269.

Grant, J.N., Halls, C., Avila, W. and Avila, G., 1977. Igneous geology and the evolution of hydrothermal systems in some sub-volcanic tin deposits of Bolivia. *Geological Society, London, Special Publications*, *7*(1), pp.117-126.

Gupta, M.L., 1981. Surface heat flow and igneous intrusion in the Cambay basin, India. *Journal of Volcanology and Geothermal Research*, *10*(4), pp.279-292.

Hesselbo, S.P., Oates, M.J. and Jenkyns, H.C., 1998. The lower Lias group of the Hebrides Basin. Scottish Journal of Geology, 34(1), pp.23-60.

Hesselbo, S.P. and Coe, A.L., 2000. Jurassic sequences of the Hebrides Basin, Isle of Skye, Scotland. IAS.

Holford, S.P., Schofield, N., Jackson, C.L., Magee, C., Green, P.F. and Duddy, I.R., 2013. Impacts of igneous intrusions on source reservoir potential in prospective sedimentary basins along the western Australian continental margin.

Huang, W.L., Longo, J.M. and Pevear, D.R., 1993. An experimentally derived kinetic model for smectite-to-illite conversion and its use as a geothermometer. Clays and Clay Minerals, 41(2), pp.162-177.

Huggett J.M. (1984) An SEM study of phyllosilicates in a Westphalian Coal Measures sandstone using back-scattered electron imaging and wavelength dispersive spectral analysis. Sediment. Geol. 40, 233-247.

Inoue, A., and Utada, M., 1983, Further investigations of a conversion series of dioctahedral mica/smectites in the Shinzan hydrothermal alteration area, northeast Japan: Clays and Clay Minerals, v. 31, p. 401-412.

Inoue, A., Utada, M., and Wakita, K., 1992, Smectite-to-illite conversion in natural hydrothermal systems: Applied Clay Sci- ence, v. 7, p. 131-145

Kastner, M., and Gieskes, J. M., 1981. Hydrothermal activity in the Guaymas Basin, Gulf of California. Trans. Am. Geophys. Union, 62:914.

Katz, A.J. and Thompson, A.H., 1986. Quantitative prediction of permeability in porous rock. Physical review B, 34(11), p.8179.

844 Kisch, H.J., 1979. Mineralogy and petrology of burial diagenesis (burial metamorphism) and incipient
845 metamorphism in clastic rocks. In Developments in Sedimentology (Vol. 25, pp. 289-493). Elsevier.

846 Klinkenberg, L.J., 1941, January. The permeability of porous media to liquids and gases. In Drilling and
847 production practice. American Petroleum Institute.

848 Lanson, B., Beaufort, D., Berger, G., Baradat, J.A., Lacharpagne, J.C. (1996): Late-stage diagenesis of
849 clay minerals in porous rocks: Lower Permian Rotliegendes reservoir off-shore of the Netherlands. J.
850 Sediment. Res., 66, 501–518.

851 Lanson, B., Beaufort, D., Berger, G., Bauer, A., Cassagnabere, A. and Meunier, A., 2002. Authigenic
852 kaolin and illitic minerals during burial diagenesis of sandstones: a review. Clay minerals, 37(1), pp.1-
853 22.

854 Leslie, A.G., Browne, M.A., Cain, T. and Ellen, R., 2016. From threat to future asset—The legacy of
855 opencast surface-mined coal in Scotland. International Journal of Coal Geology, 164, pp.123-133.

856 Macchi, L., 1987. A review of sandstone illite cements and aspects of their significance to hydrocarbon
857 exploration and development. Geological Journal, 22(4), pp.333-345.

858 Machel, H.G., 1985. Cathodoluminescence in calcite and dolomite and its chemical interpretation.
859 Geoscience Canada, 12(4) pp. 139-146

860 Machel, H.G. and Burton, E.A., 1991. Factors governing cathodoluminescence in calcite and dolomite,
861 and their implications for studies of carbonate diagenesis.

862 Mckinley, J.M., Worden, R.H. and Ruffell, A.H., 2001. Contact diagenesis: The effect of an intrusion on
863 reservoir quality in the Triassic Sherwood Sandstone Group, Northern Ireland. Journal of Sedimentary
864 Research, 71(3), pp.484-495.

865 Monreal, F.R., Villar, H.J., Baudino, R., Delpino, D. and Zencich, S., 2009. Modeling an atypical
866 petroleum system: A case study of hydrocarbon generation, migration and accumulation related to
867 igneous intrusions in the Neuquen Basin, Argentina. *Marine and Petroleum Geology*, *26*(4), pp.590-
868 605.

869 Monteiro, L.V.S., Xavier, R.P., Hitzman, M.W., Juliani, C., de Souza Filho, C.R. and Carvalho, E.D.R.,
870 2008. Mineral chemistry of ore and hydrothermal alteration at the Sossego iron oxide–copper–gold
871 deposit, Carajás Mineral Province, Brazil. *Ore Geology Reviews*, *34*(3), pp.317-336.

872 Muirhead, D.K., Bowden, S.A., Parnell, J. and Schofield, N., 2017. Source rock maturation owing to
873 igneous intrusion in rifted margin petroleum systems. Journal of the Geological Society, 174(6),
874 pp.979-987.

875 Muirhead, D.K., Duffy, M., Schofield, N., Mark, N. and Rowe, M.D., 2018. Making oil from magma.
876 Geological Society, London, Special Publications, 484, pp.SP484-8.

877 Mykura, W., 1965. White trap in some Ayrshire Coals. Scottish Journal of Geology, 1(2), pp.176-184.

878 Othman, R., Arouri, K.R., Ward, C.R. and McKirdy, D.M., 2001. Oil generation by igneous intrusions in
879 the northern Gunnedah Basin, Australia. Organic Geochemistry, 32(10), pp.1219-1232.

880 Parker, C.A., 1974. Geopressures and secondary porosity in deep Jurassic of Mississippi. AAPG Bulletin,
881 58(10), pp.2212-2212.

882 Pevear, D.R., 1999. Illite and hydrocarbon exploration. Proceedings of the National Academy of
883 Sciences, 96(7), pp.3440-3446.

884 Platt, J.D., 1993. Controls on clay mineral distribution and chemistry in the early Permian Rotliegend
885 of Germany. Clay minerals, 28(3), pp.393-416.

886 Podladchikov, Y.Y. and Wickham, S.M., 1994. Crystallization of hydrous magmas: calculation of
887 associated thermal effects, volatile fluxes, and isotopic alteration. The Journal of Geology, 102(1),
888 pp.25-45.

889 Pytte, A.M., and Reynolds, R.C., Jr., 1989, The thermal transforma- tion of smectite to illite, in
890 Naeser, N.D., and McCulloh, T.H., eds., Thermal history of sedimentary basins, methods, and case
891 histories: New York, Springer-Verlag, p. 133-140.

892 Rateau, R., Schofield, N. & Smith, M. 2013. The potential role of igneous intrusions on hydrocarbon
893 migration, West of Shetland. Petroleum Geoscience, 19, 259–272,
894 https://doi.org/10.1144/petgeo2012-035

895 Raymond A.C. and Murchison D.G. 1988. Development of organic maturation in the thermal aureoles
896 of sills and its relation to sediment compaction. *Fuel* 67: 1599-1608

897 Reeckmann, S.A., Duddy, I.R. and Gleadow, A.J., 1985. Igneous Intrusions in Porous Sandstone
898 Sequences—Widespread Thermal Effects Measured by Fission Track Annealing and Vitrinite
899 Reflectance. AAPG Bulletin, 69(2), pp.299-300.

900 Rohrman, M., 2013. Intrusive large igneous provinces below sedimentary basins: An example from the
901 Exmouth Plateau (NW Australia). JOURNAL OF GEOPHYSICAL RESEARCH: SOLID EARTH, VOL. 118,
902 4477–4487, doi:10.1002/jgrb.50298, 2013

Rossetti, L.M., Healy, D., Hole, M.J., Millett, J.M., de Lima, E.F., Jerram, D.A. and Rossetti, M.M., 2019. Evaluating petrophysical properties of volcano-sedimentary sequences: A case study in the Paraná-Etendeka Large Igneous Province. Marine and Petroleum Geology, 102, pp.638-656.

Sachsenhofer, R.F., Rantitsch, G., Ttl, C., Russegger, B. and Jelen, B., 1998. Smectite to illite diagenesis in early Miocene sediments from the hyperthermal western Pannonian Basin. Clay Minerals, 33(4), pp.523-537.

Schofield, N., Holford, S., Millett, J., Brown, D., Jolley, D., Passey, S.R., Muirhead, D., Grove, C., Magee, C., Murray, J. and Hole, M., 2015. Regional magma plumbing and emplacement mechanisms of the Faroe-Shetland Sill Complex: implications for magma transport and petroleum systems within sedimentary basins. *Basin Research*, *29*(1), pp.41-63.

Schofield, N., Jerram, D.A., Holford, S., Archer, S., Mark, N., Hartley, A., Howell, J., Muirhead, D., Green, P., Hutton, D. and Stevenson, C., 2016. Sills in sedimentary basins and petroleum systems. In Physical geology of shallow magmatic systems (pp. 273-294). Springer, Cham.

Scott, S.W. and Driesner, T., 2018. Permeability changes resulting from quartz precipitation and dissolution around upper crustal intrusions. Geofluids, 2018.

Simonet, B.R., Brenner, S., Peters, K.E. and Kaplan, I.R., 1981. Thermal alteration of Cretaceous black shale by diabase intrusions in the Eastern Atlantic—II. Effects on bitumen and kerogen. *Geochimica et Cosmochimica Acta*, *45*(9), pp.1581-1602.

Singurindy, O., Berkowitz, B. and Lowell, R.P., 2004. Carbonate dissolution and precipitation in coastal environments: laboratory analysis and theoretical consideration. Water Resources Research, 40(4).

Senger, K., Planke, S., Polteau, S., Ogata, K. and Svensen, H., 2014. Sill emplacement and contact metamorphism in a siliciclastic reservoir on Svalbard, Arctic Norway. *Norwegian Journal of Geology/Norsk Geologisk Forening*, *94*

Senger, K., Millett, J., Planke, S., Ogata, K., Eide, C.H., Festøy, M., Galland, O. and Jerram, D.A., 2017. Effects of igneous intrusions on the petroleum system: a review. First Break, 35(6), pp.47-56.

Smallwood, J.R., Harding, A., Varming, T. and Ziska, H., 2009. New seismic imaging methods, dating, intrusion style and effects of sills: a drilled example from the Faroe-Shetland Basin. In Faroe Islands Exploration Conference: Proceedings of the 2nd Conference. Annales Societatis Scientiarum Færoensis, Tórshavn, Suppl (Vol. 50, pp. 104-123).

Sydnes, M., Fjeldskaar, W., Grunnaleite, I., Løtveit, I.F. and Mjelde, R., 2019. The Influence of Magmatic Intrusions on Diagenetic Processes and Stress Accumulation. Geosciences, 9(11), p.477.

934 Tanikawa, W. and Shimamoto, T., 2009. Comparison of Klinkenberg-corrected gas permeability and
935 water permeability in sedimentary rocks. International Journal of Rock Mechanics and Mining
936 Sciences, 46(2), pp.229-238.

937 Taylor, H.P., 1974. The application of oxygen and hydrogen isotope studies to problems of
938 hydrothermal alteration and ore deposition. Economic geology, 69(6), pp.843-883.

939 Thomaz Filho, A., Mizusaki, A.M.P. and Antonioli, L., 2008. Magmatism and petroleum exploration in
940 the Brazilian Paleozoic basins. *Marine and petroleum geology*, *25*(2), pp.143-151.

941 Thompson, A.J.B., Thompson, J.F.H. and Dunne, K.P.E., 1996. Atlas of alteration: a field and
942 petrographic guide to hydrothermal alteration minerals. Geological Association of Canada. Mineral
943 Deposits Division, 119.

944 Townsend, M, R., 2018. Modelling thermal pressurization around shallow dikes using temperature-
945 dependant hydraulic properties: implications for deformation around intrusions. Journal of
946 Geophysical Research: Solid Earth, 123:311-323

947 White, R. and McKenzie, D., 1989. Magmatism at rift zones: the generation of volcanic continental
948 margins and flood basalts. *Journal of Geophysical Research: Solid Earth*, *94*(B6), pp.7685-7729.

949 White, S.H., Huggett, J. M., Shaw, H. F., 1985 Electron-optical studies of phyllosilicate intergrowths in
950 sedimentary and metamorphic rocks. Mineralogical magazine 49:413-423.

951 Wilkinson, M., Haszeldine, R.S. and Fallick, A.E., 2014. Authigenic illite within northern and central
952 North Sea oilfield sandstones: evidence for post-growth alteration. Clay Minerals, 49(2), pp.229-246.

953 Wilson, M.E., Evans, M.J., Oxtoby, N.H., Nas, D.S., Donnelly, T. and Thirlwall, M., 2007. Reservoir
954 quality, textural evolution, and origin of fault-associated dolomites. AAPG bulletin, 91(9), pp.1247-
955 1272.

956 Wright, V.P. and Tucker, M.E. eds., 2009. Calcretes (Vol. 44). John Wiley & Sons.

957

958

959

960

961

962

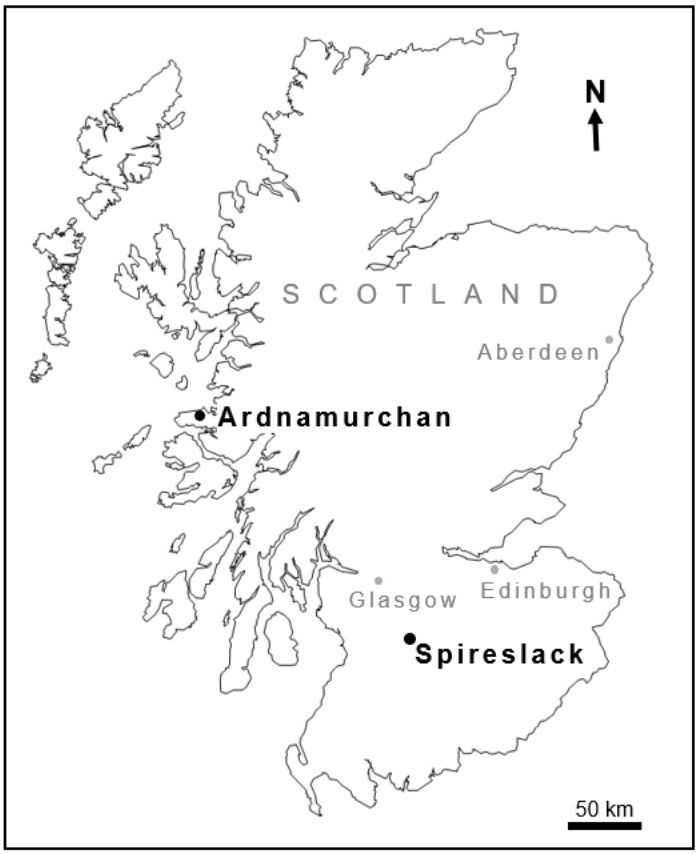

Fig. 1. Location map highlighting sample localities: Ardnamurchan (calcareous sandstone) and Spireslack (clay rich sandstone).

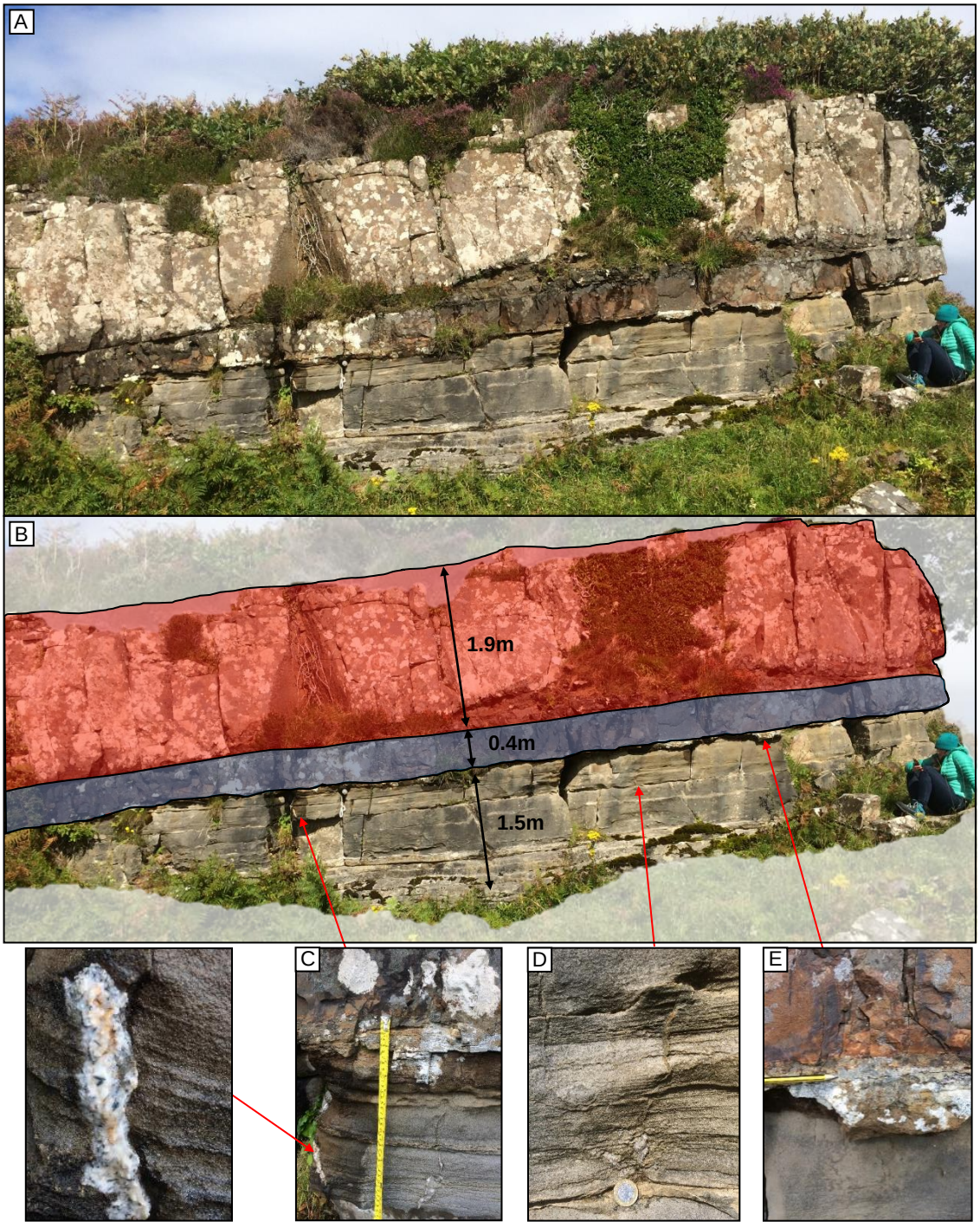

Fig. 2. Ardnamurchan, calcareous sandstone sample site: (A) Outcrop photo of Ardnamurchan compound sill (2.3 m) and calcareous sandstone exposure (1.5m), (B) annotated outcrop photo with intrusion dimensions, (C,D) calcareous sandstone and calcite veining most prominent in proximity to the intrusion with fractures observed vertical and horizontal to intrusion (E) Intrusion (top of image) with wavy contact zone compromised of brown friable sandstone.

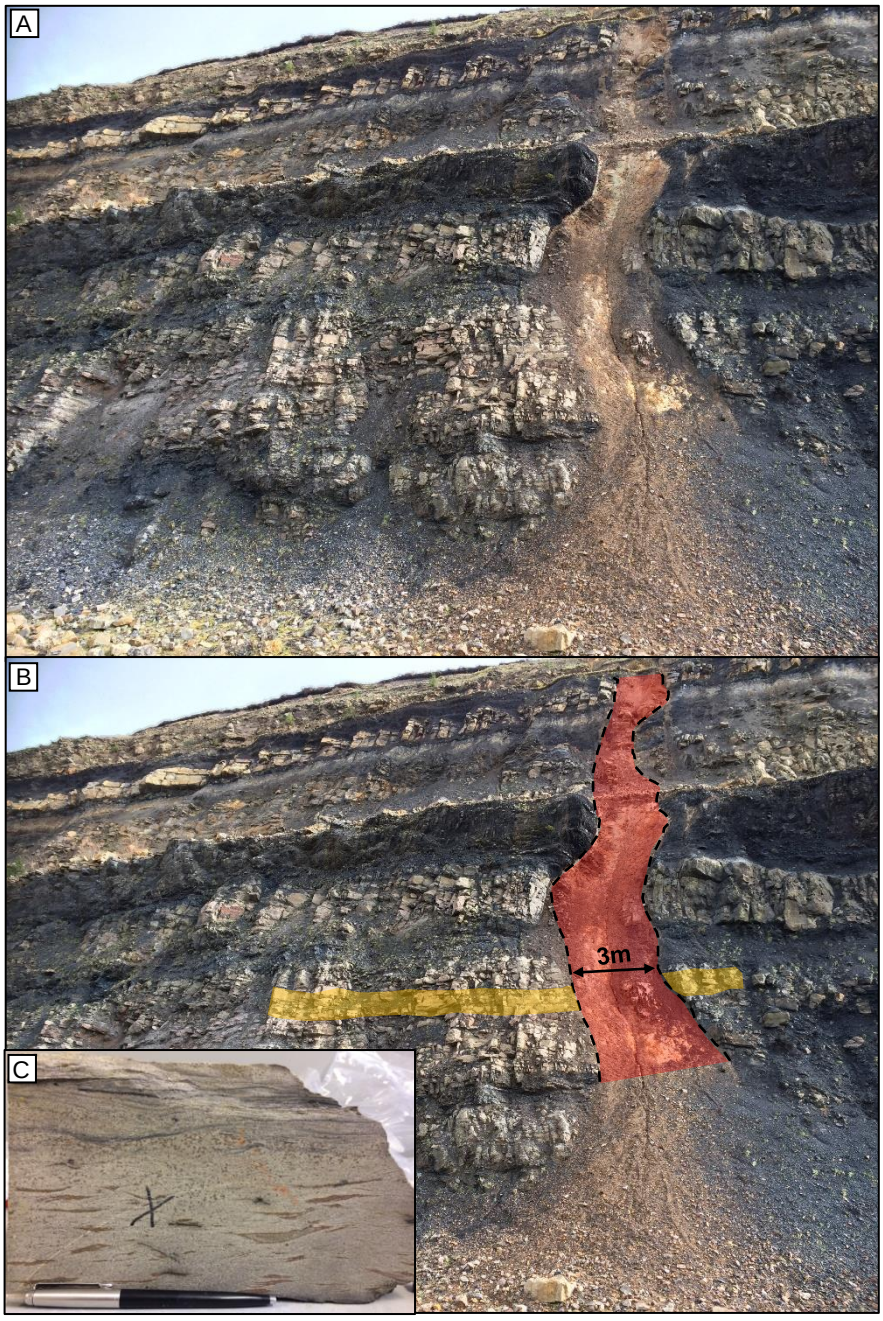

Fig. 3. Spireslack, clay rich sandstone sample site (NS 74817 30472): (A) 80m cliff section comprised of Carboniferous fluvial sandstones, shales, coals and limestones. (B) Annotated field photo of the southwest wall of the Spireslack main void. Dyke highlighted in red on the quarry wall and the sampled clay rich sandstone bed highlighted in yellow. (C) Clay rich sandstone example showing asymmetrical current ripples with slight mud draping present along with cross laminations.

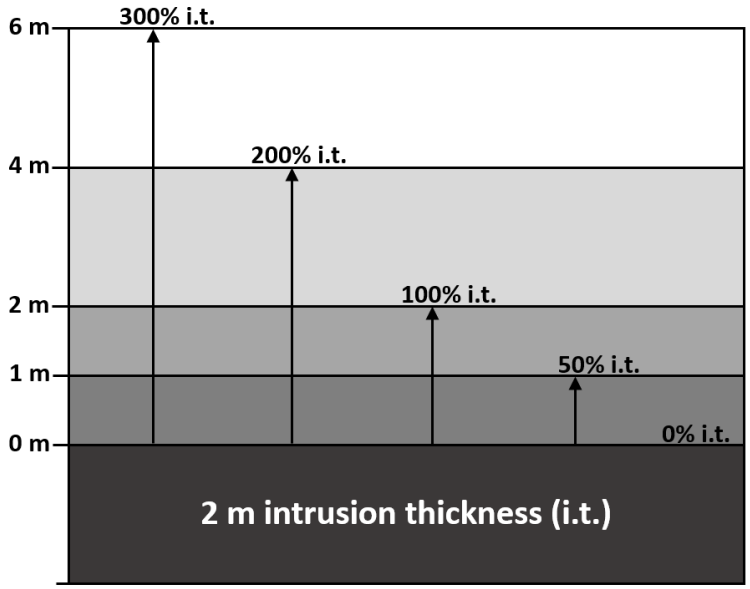

Fig. 4. Distance away from intrusion described as a percentage of intrusion thickness (% i.t.). Used for comparing intrusions of different sizes and orientations.

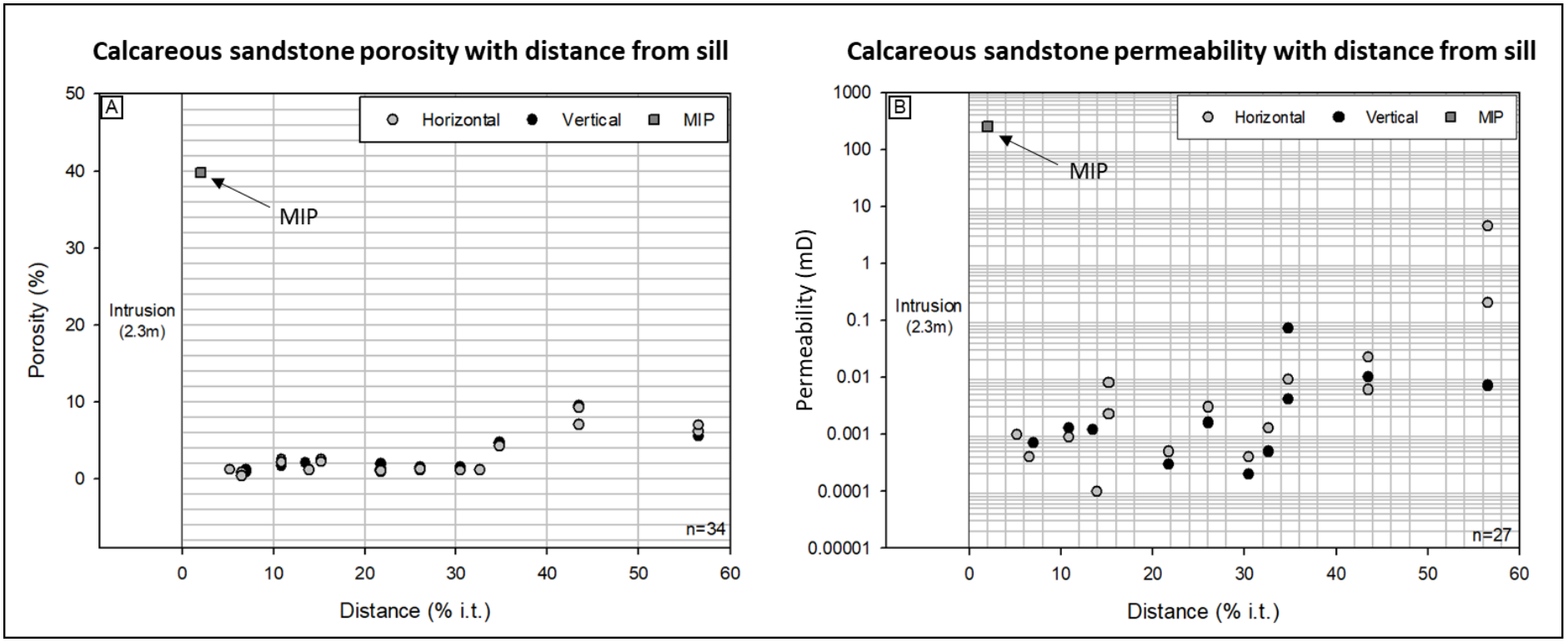

Fig. 5. Graphs showing changing reservoir quality properties of calcareous sandstone sampled from around an intrusion in Ardnamurchan: (A) Porosities measured on core plugs at ambient pressures using He permeant. Distance from contact expressed as % intrusion thickness. Porosity first decreases towards sill at 35 % i.t. and then an increased porosity of 38.9 % measured from mercury injection porosimetry (MIP) at 0% i.t.. (B) Core plug permeabilities measured using N_2 as pore fluid. The permeability reduces towards the intrusion. Contact zone shows increased permeability calculated from MIP using the Katz-Thompson model.

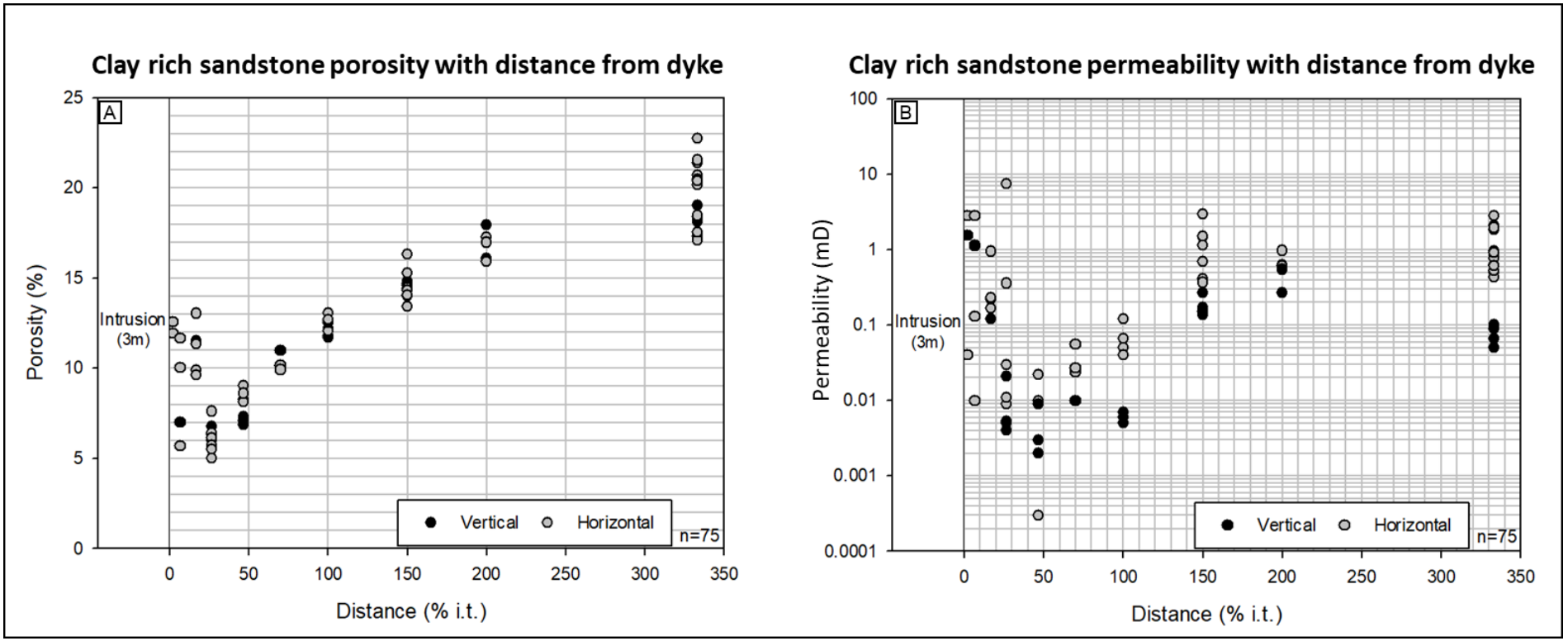

Fig. 6. Clay rich sandstone, core plug porosity and permeability: (A) Graph showing porosities measured on core plugs at ambient pressures using He. Close to the dyke, porosities decrease by up to 20 %. Porosities are more variable at the dyke contact zone. (B) Core plug permeabilities measured using N_2 as permeant. The permeability reduces towards the intrusion, with an increase noted at contact zone.

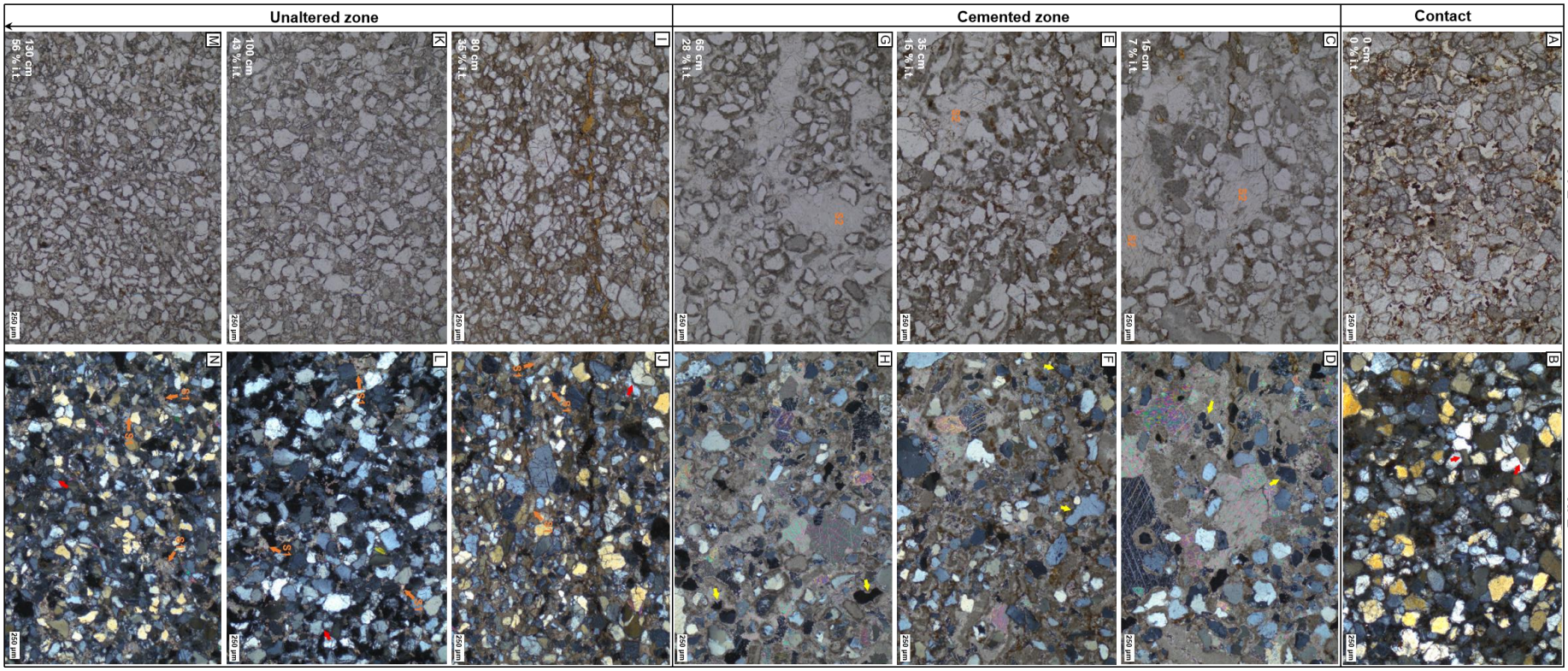

Fig. 7. Calcareous sandstone, Petrographic sections from 0-56% i.t.: (A,B) Contact zone (0 % i.t.) with pore spaces containing dark brown amorphous iron-rich oxides. No calcite cement present at contact. Tight packing of quartz grains with point contacts, chemical compaction textures (red arrows) and grain microfractures. (C-H) Cemented zone (7-28 % i.t.), large sparry calcite (S2) crystals (50-500 µm) and darker grey/brown micrite filling pore spaces between grains. Grain contacts predominantly point but floating textures where heavily cemented. Irregular edges of grain dissolution (yellow arrow), carbonate grains (peloids) seen as dull brown micritic spheres. (I-J) Unaltered zone (35-56 % i.t.), predominantly quartz grains with point contacts between grains with some chemical compaction textures (red arrows), dull brown micrite cement surrounds grains and small sparry calcite (S1) crystals (≥50 µm) filling intergranular porosity. Increase in visible porosity (low relief, opaque). * [Light brown patches seen (7-56 % i.t.) are an artefact due to residual carbon coating from SEM not iron oxide].

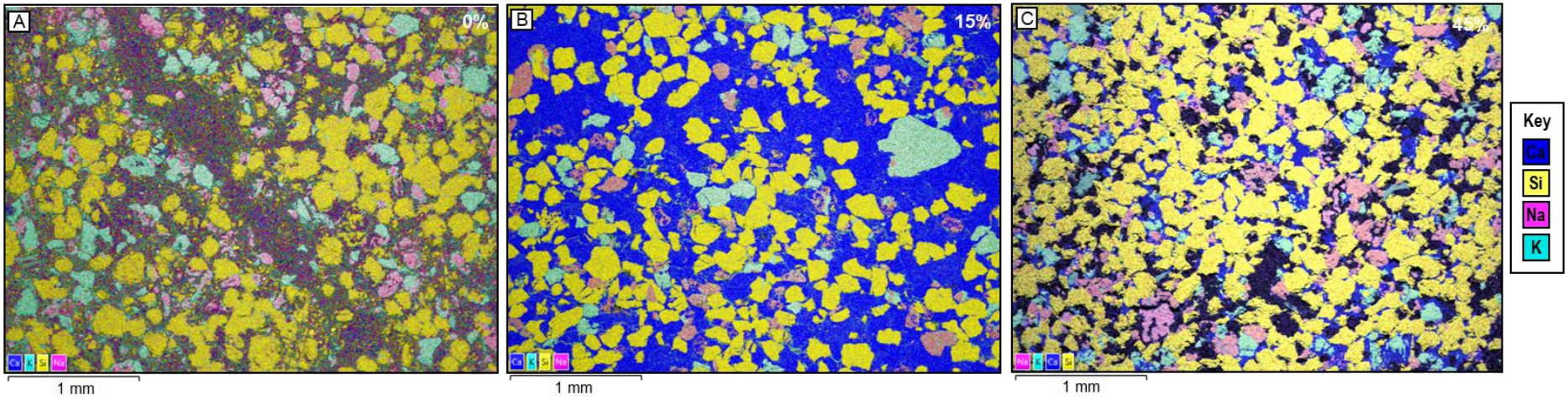

Fig. 8. Calcareous sandstone, EDS maps displaying individual elemental layers. Colour and brightness depend on the chemical composition and concentration of the host rock material. Selected elements layered onto false coloured elemental maps include calcium (dark blue), silica (yellow), potassium (light blue), sodium (magenta) no elements (black). The grains and cements interpreted from elemental compositions are quartz (yellow), sodium feldspar (pink), k-feldspar (light blue), carbonate grains and cements (dark blue) and porosity (black). (A) Contact zone (0% i.t.) contains high porosity (black), with no carbonate (dark blue/calcite) material present. (B) Mid zone (7-35 % i.t.) is highly cemented with a high volume of calcium material (allochems and cements) filling a significant portion of the rock with little visible porosity. (C) More distal to the intrusion (from 35-56 % i.t.), porosity increases seen as black with less carbonate material present.

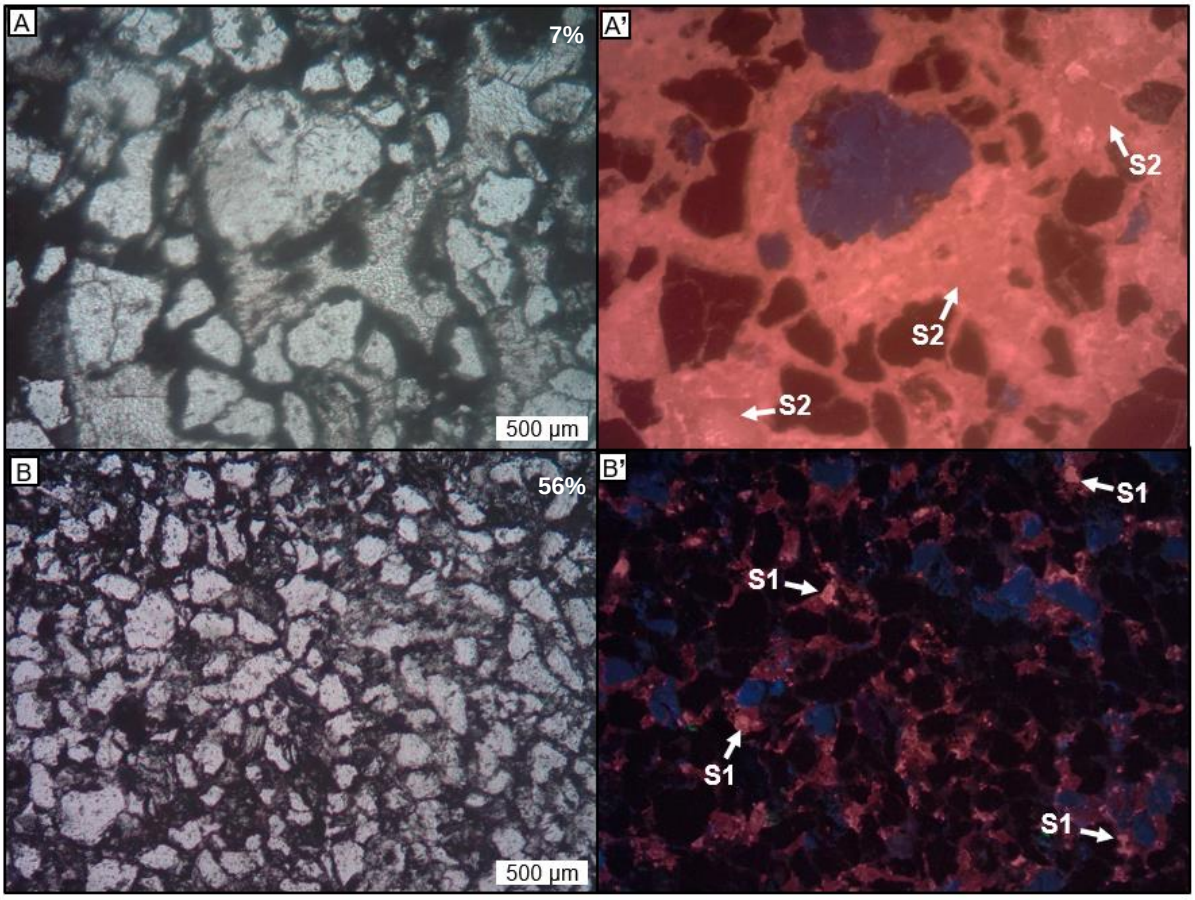

Fig. 9. Calcareous sandstone, cathodoluminescence analysis: (A,B) PPL (plane-polarised light) image (A',B') CL (cathodoluminescence) image displaying black (quartz), blue (feldspar) and varying brightness of red (carbonates). (A+A') At close proximity to the intrusion (7-28 % i.t.) CL images show large sparite crystals (>250 µm) with dull luminescence (S2) surrounded by micrite. Micrite appears bright red in CL and dull brown in PPL. Quartz and feldspar grains occasionally display a dull brown carbonate rim in CL around grain edge. (B) With increasing distance from the intrusion (>28 % i.t.) sparite crystals appear bright and smaller (>100 µm) (S1) with a duller micrite surrounding.

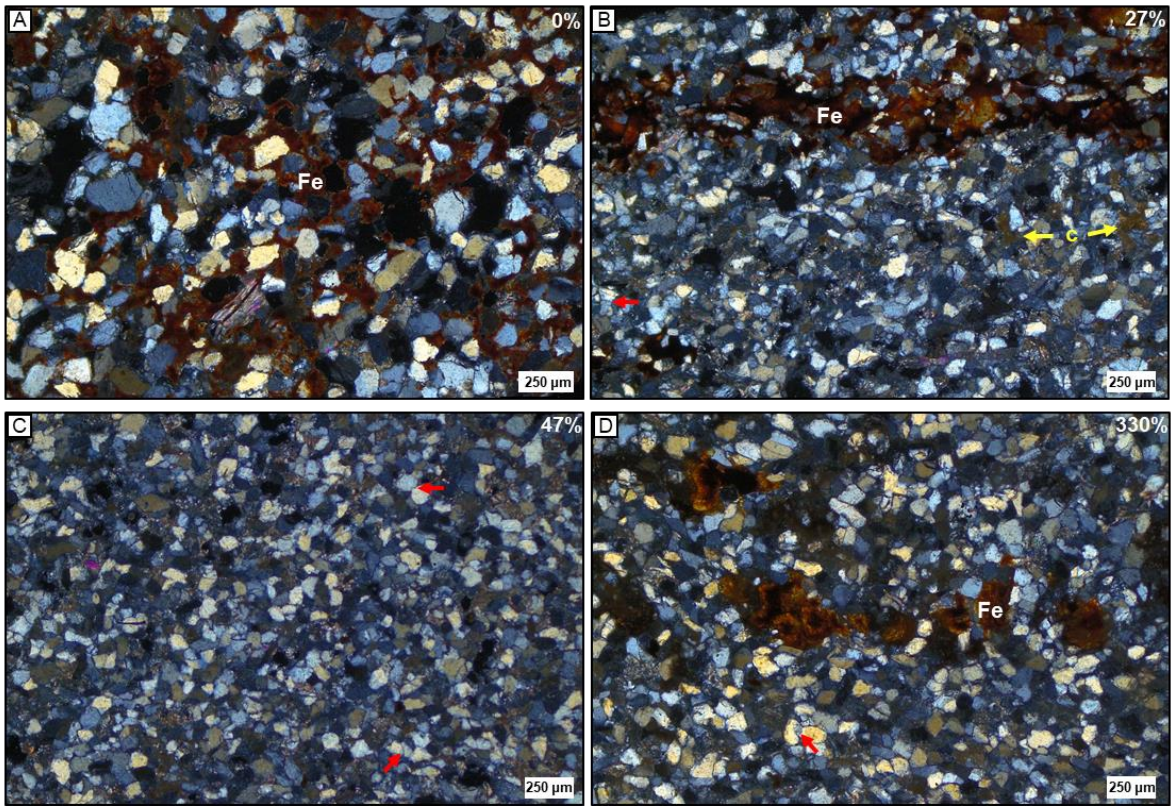

Fig. 10. Clay rich sandstone (XPL images): Representative microscopy images of clay rich sandstone from contact to background (0-330 % i.t.). Samples are predominantly quartz rich with a dusty brown clay matrix. Majority of grains display point contacts, occasional concave-convex contacts and irregular grain edges indicating clay induced chemical compaction. (A) At the contact (0 % i.t.) grains are coated and pores filled by dark brown iron oxides (Fe). A dusty lighter brown pore filling material is still visible indicating clay content but often hidden by the darker iron oxides. (B) 27 % i.t. from the intrusion the predominant pore filling materials are illite and kaolinite clays (c) (dusty brown). The iron oxide (Fe) previously prevalent at the contact is limited to fractures and high permeability pathways. (C) 47 % i.t. as previous, predominant composition of quartz grains and pore filling clays. Opaque spaces are either porosity or grains plucked during thin-section creation. (D) Background sample (330 % i.t.). Crystalline spherulitic siderite (Fe) occurring parallel to bedding but not grain coating as seen at contact zone. Predominant pore filling material dusty brown clays.

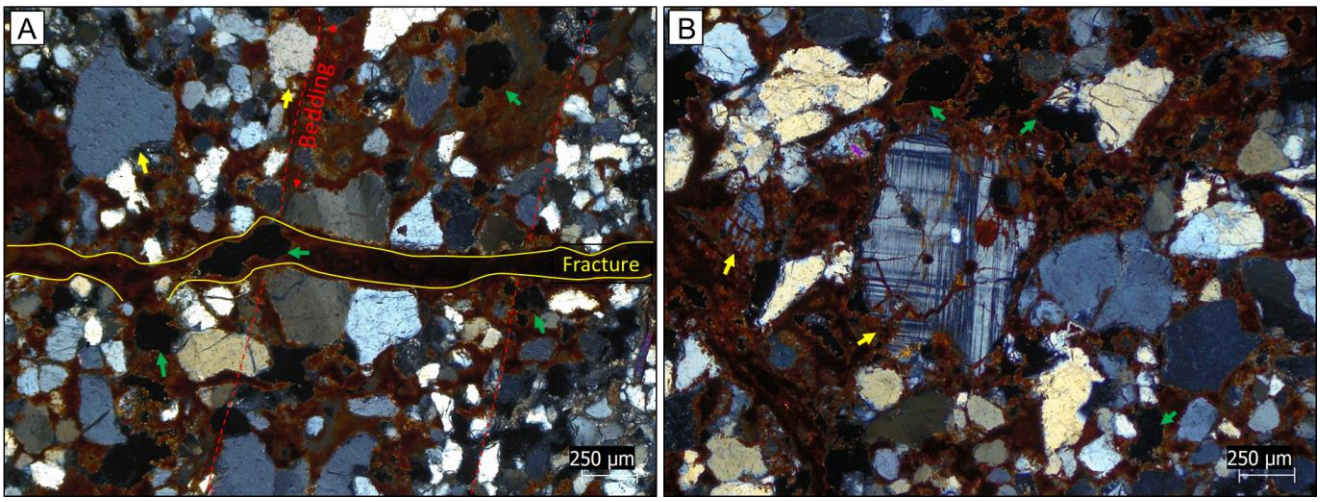

Fig 11. Clay-rich sandstone, contact zone sample (0 % i.t.), XPL images: Fractures and dissolved grains develop secondary porosity (green arrows) with fractures observed splitting grains. Yellow arrows identify angular embayment's and serrated edges indicating grain dissolution. Most grains contacts are point. Floating textures are seen in vicinity to the fracture and concavo-convex contacts are also observed. Fractures and intergranular porosity have been coated with iron oxide.

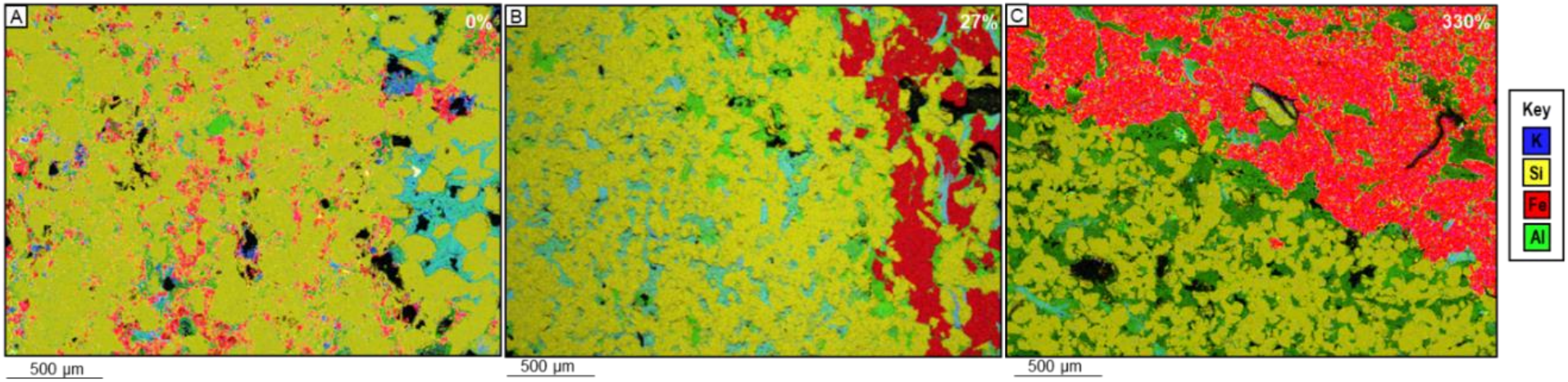

Fig. 12. Clay rich sandstone, EDS maps: selected element layers include; potassium (blue), silica (yellow), iron (red) and aluminium (green). Amorphous iron oxides highlighted in red are prominent within intergranular pore space at contact but not more distally. Red within B and C is present due to coarse spherulitic siderite parallel to bedding. Pore filling clay type can be observed with kaolinite (green) and potassium rich illite (blue). (A) Contact (0 % i.t.) shows large aggregate of illite/mica to the right whilst most intergranular porosity is filled with iron (red) and kaolinite (green). (B) At 27 % i.t. proportion of potassium occurring between silica rich grains increases indicating illite. Both kaolinite and illite are interpreted within pores. (C) Distal unaltered sample 330 % i.t. shows predominant pore filling material to be potassium poor kaolinite with detrital micas highlighted in blue. Iron rich band represents large spherulitic siderite lense.

Clay Fraction %				
Distance (i.t. %)	**0%**	**27%**	**47%**	**330%**
Illite	13.5	25.7	40.9	11.5
Illite/smectite	0	24.6	23.7	9.7
Kaolinite	76	42.1	30.9	77
Quartz	7.4	7.7	4.5	1.8
Siderite	3.1	0	0	0
Clay Volume	6.4	5.8	4.7	10
Illite crystallinity	Poor	Moderate		Poor
Kaolinite crystallinity	Moderate			Well
Whole rock %				
Illite + mica	5.4	15.7	11.1	10.6
Illite/smectite	0	1.4	1.1	0
Kaolinite	6.4	2.8	5.4	11.7
Quartz	77.2	79.5	80.3	69.7
Siderite	8.1	0	0.9	7.5
Other	2.9	0.6	1.2	0.5

Table. 1. Clay rich sandstone, clay fraction and whole rock analyses performed on four samples with increasing distance from intrusion. Samples chosen to represent contact, reduced zone and unaltered sample based on SEM observations. Increase in illite within the reduced zone 27 % i.t. and 47 % i.t. compared to unaltered sample at 330 % i.t. Quartz content increases towards intrusion and siderite is present at contact.

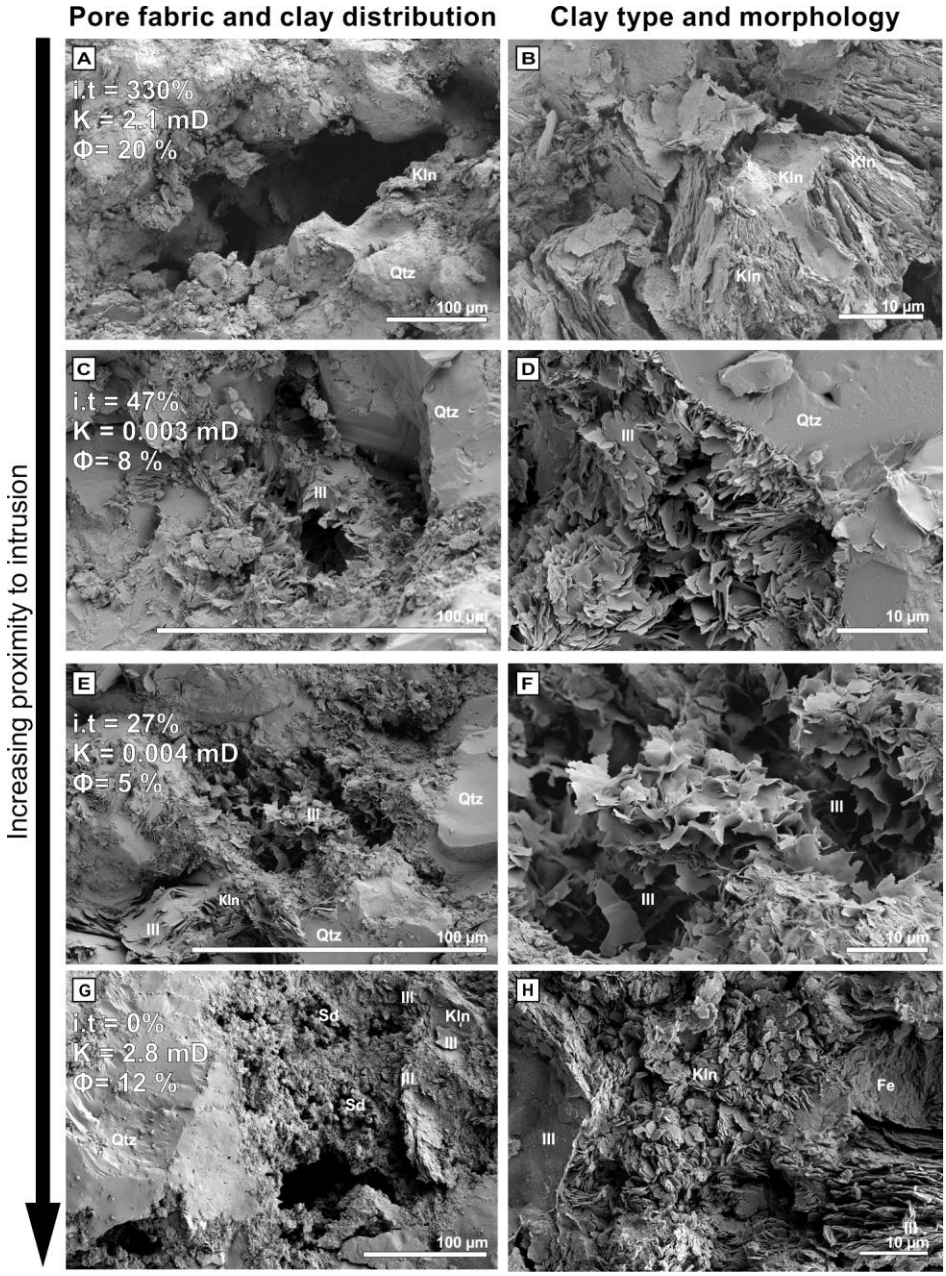

Fig. 13. Clay rich sandstone, secondary electron (SE) images showing changing microstructure and mineralogy with distance to intrusion: (A) SE image of clay rich sandstone (unaltered sample) located 10 m (330 % i.t.) from intrusion shows a porous fabric with large irregular shaped pores developed through dissolution of feldspars. (B) Predominant clay is kaolinite showing typical vermicular shape with booklets ranging from 1-20µm. (C) SE image of clay rich sandstone located 140 cm (47 % i.t.) from the intrusion shows well formed illite growing into pores. Kaolinite clays remain present with similar grain sizes to illite, but have been largely broken down to individual books rather than well developed vermiforms. (D) Illite plates occur as pore filling and pore rimming clay. Quartz growth into illite at grain contact. (E). Under 140 cm (<47 % i.t.) from the intrusion, platy aggregates of illite coat quartz grains extensively, clogging up intergranular and secondary pores and reducing permeability by four orders of magnitude. (F) Magnification of E highlighting well-formed curved flakes of illite 2-15 µm filling into secondary porosity. (G) At contact 0cm (0 % i.t.) siderite is seen as fine nodular cement coating grains and filling pore spaces. Increase in visible porosity. (H) Kaolinite 1-2 µm fills pores, illitised kaolinite (bottom right), shows that kaolinite vermiform structure has been preserved. Illitised vermiform includes bands of siderite (Fe) 10µm thick.

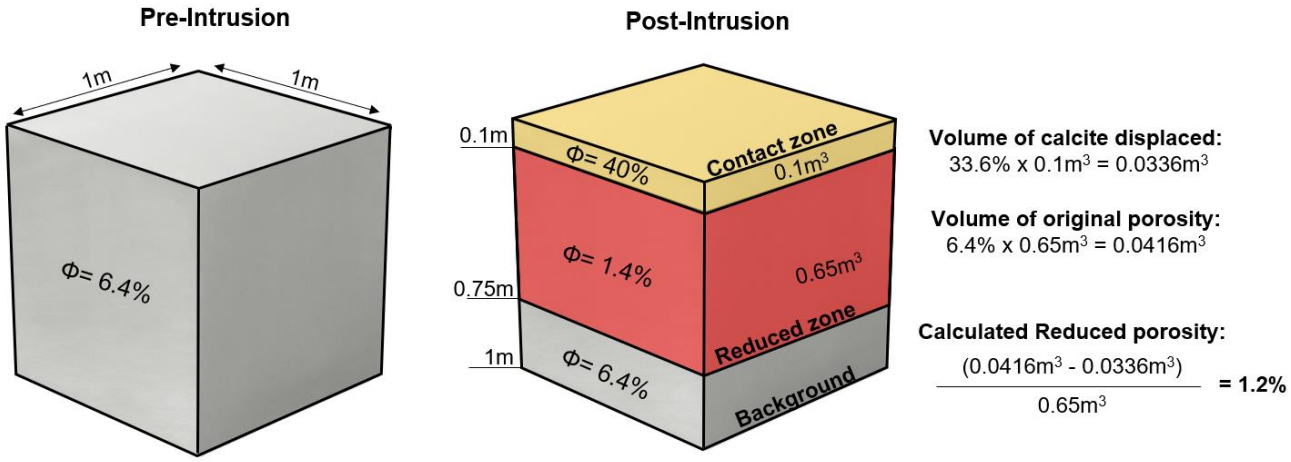

Fig. 14. Calcareous sandstone, porosity calculation estimating porosity change based on redistribution of calcite cements. Left box represents sandstone prior to intrusion with an original porosity of 6.4 % (assumed from unaltered sample). Right box (post-intrusion) showing high porosity contact zone in yellow and adjacent reduced porosity zone in red giving the measurements from core plug porosity. Volume of calcite displaced calculated from the porosity generated at the contact (40% - 6.4% = 33.6%) multiplied by the rock volume of the contact zone. Porosity calculation shows removed calcite reduces porosity to 1-2 % in the reduced zone (red) matching measured results.

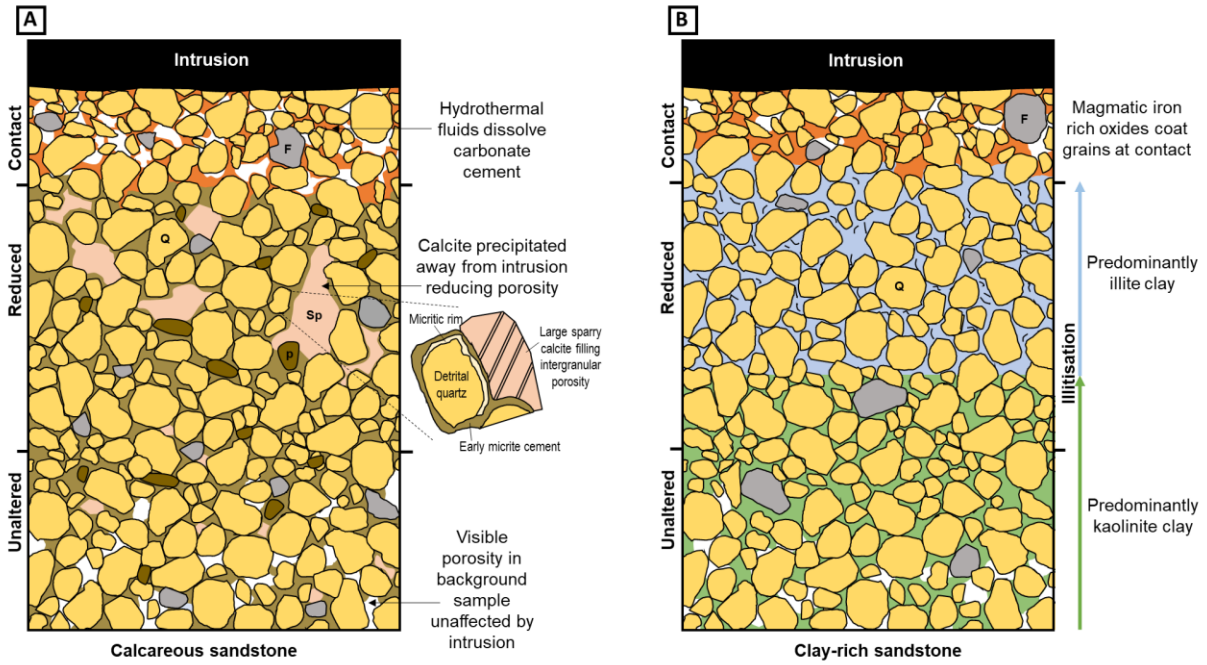

Fig. 15. Schematic diagram representing the effect of igneous intrusions on (A) calcareous sandstone and (B) clay rich sandstone. Q= quartz grains, F= feldspar grains, Sp= sparry calcite cement, p= peloids/carbonate grains. (A) Calcareous sandstone displaying an increased porosity-permeability at the contact zone due to the removal of carbonate cements (buff brown) by hydrothermal fluids and precipitation of iron oxides (orange). Below the contact zone (reduced zone) the porosity decreases where calcite is precipitated (Sp) which is interpreted to be the remobilised cements lost from the contact. With increasing distance from the intrusion an increase in visible porosity (white) is observed within the unaltered samples unaffected by the intrusion. (B) Clay rich sandstone background samples contain predominantly kaolinite pore filling material (green). With increasing proximity to the intrusion kaolinite becomes unstable and illite (blue) forms at temperatures >130 ^{o}C. The contact zone shows a slight increase in porosity-permeability (white) due to hydrothermal fluids flushing potassium bearing fluids further away and precipitating iron oxides (orange) which coated grains restricting illitisation.